NUSC Technical Report 5263

Dynamic Nonlinearities in Piezoelectric Sonar Ceramics

Charles L. LeBlanc
Russell W. Dunham
Timothy D. Sullivan
Special Projects Department

27 December 1976

NUSC
NAVAL UNDERWATER SYSTEMS CENTER
Newport, Rhode Island • New London, Connecticut

PREFACE

This research was performed under NUSC Project No. A-700-19, "Ferroelectric Nonlinearities in Transducer Ceramics," Principal Investigator, C. L. LeBlanc (Code 316), and Navy Project No. RR02206, Program Manager, Dr. A. M. Diness (Code 471), Metallurgy Program, ONR.

The Technical Reviewer for this report was J. W. Frye (Code 401).

The authors are grateful to W. H. Gladu (Code 316) for his help in establishing the measurement system, to Dr. C. H. Sherman (Code 316) and Dr. R. S. Woollett (Code 316) for their constructive criticism and support, and to Dr. Diness for sponsoring this work.

REVIEWED AND APPROVED: 27 December 1976

R. W. Hasse
Head: Special Projects Department

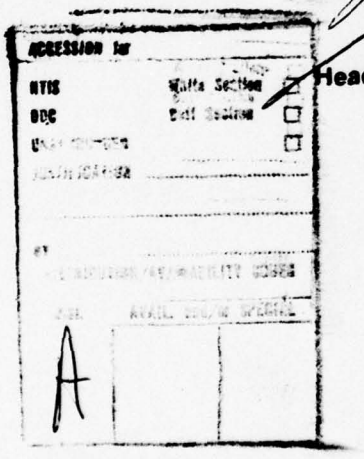

The authors of this report are located at the New London Laboratory, Naval Underwater Systems Center, New London, Connecticut 06320.

UNCLASSIFIED

SECURITY CLASSIFICATION OF THIS PAGE (When Data Entered)

REPORT DOCUMENTATION PAGE

READ INSTRUCTIONS BEFORE COMPLETING FORM

(14) NUSC TR-5263 ✓

1. REPORT NUMBER: NUSC TR-5263 ✓
2. GOVT ACCESSION NO.:
3. RECIPIENT'S CATALOG NUMBER:

4. TITLE (and Subtitle): (6) DYNAMIC NONLINEARITIES IN PIEZOELECTRIC SONAR CERAMICS.

5. TYPE OF REPORT & PERIOD COVERED: (9) Technical Report

6. PERFORMING ORG. REPORT NUMBER:

7. AUTHOR(s): (10) Charles L. LeBlanc, Russell W. Dunham, and Timothy D. Sullivan

8. CONTRACT OR GRANT NUMBER(s):

9. PERFORMING ORGANIZATION NAME AND ADDRESS:
Naval Underwater Systems Center ✓
New London Laboratory
New London, CT 06320

10. PROGRAM ELEMENT, PROJECT, TASK AREA & WORK UNIT NUMBERS:
~~A-700-19~~ 61153N
(16) RR02206 ✓

11. CONTROLLING OFFICE NAME AND ADDRESS:
Office of Naval Research
Arlington, VA 22217

12. REPORT DATE: (11) 27 December 1976

13. NUMBER OF PAGES: 68 (12) 64p.

14. MONITORING AGENCY NAME & ADDRESS (if different from Controlling Office):

15. SECURITY CLASS. (of this report): UNCLASSIFIED

15a. DECLASSIFICATION/DOWNGRADING SCHEDULE:

16. DISTRIBUTION STATEMENT (of this Report)

Approved for public release; distribution unlimited.

17. DISTRIBUTION STATEMENT (of the abstract entered in Block 20, if different from Report)

18. SUPPLEMENTARY NOTES

19. KEY WORDS (Continue on reverse side if necessary and identify by block number)

20. ABSTRACT (Continue on reverse side if necessary and identify by block number)

A measurement system was established to probe the nonlinear response of piezoelectric ceramic rings driven at their fundamental "hoop-mode" resonance frequencies with progressively increasing electrical driving fields, up to and including the field at which fracture occurred. Initial measurements indicated that Navy Type-I ceramic materials from different suppliers differed substantially in output strain level (a 14 percent difference in strain amplitude for dimensionally similar rings at 8 kV/m) and fracture strength as well as in the onset and degree of

over

DD FORM 1 JAN 73 1473 EDITION OF 1 NOV 65 IS OBSOLETE
S/N 0102-014-6601 |

UNCLASSIFIED 405 918
SECURITY CLASSIFICATION OF THIS PAGE (When Data Entered)

6pg

20. (Cont'd)

nonlinear response. The measurements also included input current, resonance frequency, and mechanical quality factor versus electric driving field.

A nonlinear theory for interpretation of the measured data was developed for the piezoelectric ring, and the resulting differential equation of motion was programmed in an analog computer. The output plots showed nonlinear "jump" phenomena in the frequency region about resonance as well as "beat" phenomena in the current envelope response, both of which were observed experimentally. Therefore, analog computer techniques may be the most convenient means of interpreting and understanding the nonlinear behavior of ceramic transducer materials.

TABLE OF CONTENTS

LIST OF ILLUSTRATIONS

LIST OF TABLES

DYNAMIC NONLINEARITIES IN PIEZOELECTRIC SONAR CERAMICS

INTRODUCTION

Transducers for Navy sonar systems are often operated at such high power levels that the polarized ferroelectric ceramics in them begin to exhibit nonlinear behavior. The degree of nonlinearity depends on such factors as electric field level, dynamic mechanical stress level, and static bias stress as well as on temperature and time. The overall influence on the ceramic in a practical transducer is a combination of these factors and, as such, presents a complex situation for interpretation of nonlinear behavior. To alleviate this complex situation, experiments are usually designed to treat the various influential factors independently, and measurement procedures and representative experimental data for ferroelectric nonlinearities in ceramics can be found in several references.[1,2]

If transducer ceramics are to be operated at their ultimate power capacities, substantial nonlinear effects will have to be tolerated and a nonlinear design theory will be needed. The alternative is to reduce the nonlinear effects in currently used ceramics (for example, by prestressing) or to develop new improved ceramic materials that are linear over a wider range of transducer operating conditions. In either case, it is essential to develop a better understanding -- through experimentation and theoretical analysis -- of the nonlinear behavior of ceramics and to somehow relate the findings to the microscopic structure of the ceramic materials.

The investigation of nonlinear behavior in piezoelectric ceramics has been, for many years, an intriguing area of research but without fruition. Even with the use of acoustic dummy-load techniques, where practical design data for transducer ceramics may be obtained under simultaneous application of high electric field and high stress, both static and dynamic, the basic underlying mechanisms responsible for the nonlinear behavior are not well understood. For example, a nonlinear "jump" phenomenon has been detected[3] in ferroelectric ceramics, but methods for explaining the behavior are nil even though the behavior of the nonlinear oscillator is well known.[4] This disparity is attributable to the fact that very little simplified nonlinear theory applicable to the low frequency domain (as opposed to high frequency nonlinear theory that can be validated by ultrasonic measurements) and of practical utility for transducer ceramics has been adapted to the ferroelectric ceramic materials. A simplified mathematical approach is preferred as a tool at present because of the complexity that would exist in analyzing large transducer arrays if a continuum-physics approach[5] were used.

Therefore, the initial efforts in this study were directed at developing a dynamic nonlinear theory for a simple structure -- a thin-walled, axially (longitudinally) polarized ceramic ring that undergoes essentially a single-degree-of-freedom vibration. This particular shape was chosen for convenience of measurement as well as for ease of applying nonlinear theory.

Results of the investigation are presented in terms of measurement procedure, representative data, experimental data and interpretation, and nonlinear theoretical analysis.

MEASUREMENT PROCEDURE

The intent was to provide a measurement system capable of determining simultaneously as many dynamic variables as possible for piezoelectric ceramic specimens driven electrically at their fundamental resonance frequencies in a "free" condition (minimum mechanical damping) in discrete steps from low-level values up to and including the value at which fracture of the specimens occurs.

SAMPLES

The piezoelectric material initially chosen for investigation was Navy Type-I[6] ceramic, a hard lead-zirconate-titanate composition, because of its extensive usage in present-day, high power sonar transducers. The ceramic specimens were in the form of thin-walled rings with dimensions

Outside diameter	2.50 in. (63.5 mm)
Wall thickness	0.25 in. (6.35 mm)
Height	0.50 in. (12.7 mm)
Ratio of height to mean radius	0.444
Ratio of outside diameter to wall thickness	10.

The dimensions are sufficient[7] to ensure pure hoop-mode resonance of the ring, and, therefore, the rings may be considered to be undergoing a single-degree-of-freedom vibration.

The ring samples measured in this investigation had previously been measured[8] to determine compliance with the standard low-level parameter values for the material.[6]

ELECTRICAL CONNECTIONS

The rings have fired-on silver electrodes on the upper and lower surfaces and are axially polarized. The driving voltage is applied to

the rings through thin (0.005 in. (127 μm) diameter) single-strand wires. The connections were initially made by simply soldering the wire leads to the silver electrodes, but that arrangement appeared to cause localized heating effects (two trial rings fractured approximately at the solder joints) and to lead to separation of the connections at large displacement amplitudes. The final method of making the connections therefore consisted of soldering the electrical lead to a small copper tab, cementing the tab to either the upper flat electrode (high electric potential side) or the curved outside surface of the ring near the bottom electrode (low electric potential side), and ensuring electrical continuity by applying air-dry silver paint between the tab and the silver electrode surface. (A tab or electrical lead could not be connected directly to the bottom electrode surface of the ring because there was insufficient room between the surface and the aluminum base of the gas-bearing suspension system, which also served as electrical ground.)

SUSPENSION

The rings were mounted freely on a gas-bearing suspension system[9] (see figure 1) to minimize mechanical damping during the dynamic measurements; the assembly is specifically designed for piezoelectric ceramic rings with an inside diameter slightly larger than the central support. Vertical levitation is provided by a precision circular gas channel in the aluminum bearing base, and horizontal stability is provided by a circumferential gas channel located in the nylon cylindrical support on top of the base.

Each channel was fed from its own gas reservoir and pressure was applied to the rings via three small orifices, about 0.008 to 0.010 in. (200 to 250 μm) in diameter and spaced 120° apart in each channel. Two separate regulators (fed from a single nitrogen supply tank) controlled the pressure in the gas reservoirs and were set at 7 lbf/in.^{2} and 9 lbf/in.^{2} (48 and 62 kN/m^2) for the levitation and stabilizing channels, respectively; these settings produced the best ring stability.

The vertical suspension of a single ring (weight approximately 0.1 kg) was approximately 0.0005 to 0.0010 in. (12.7 to 25.4 μm) above the aluminum base. This was the reason the lower electrical lead was placed on the side of the ring and not directly on the lower silver electrode. The gap spacing between the inside surface of the ring and the nylon support ranged from 0.005 to 0.010 in. (127 to 254 μm), depending on the degree of eccentricity of the ceramic ring.

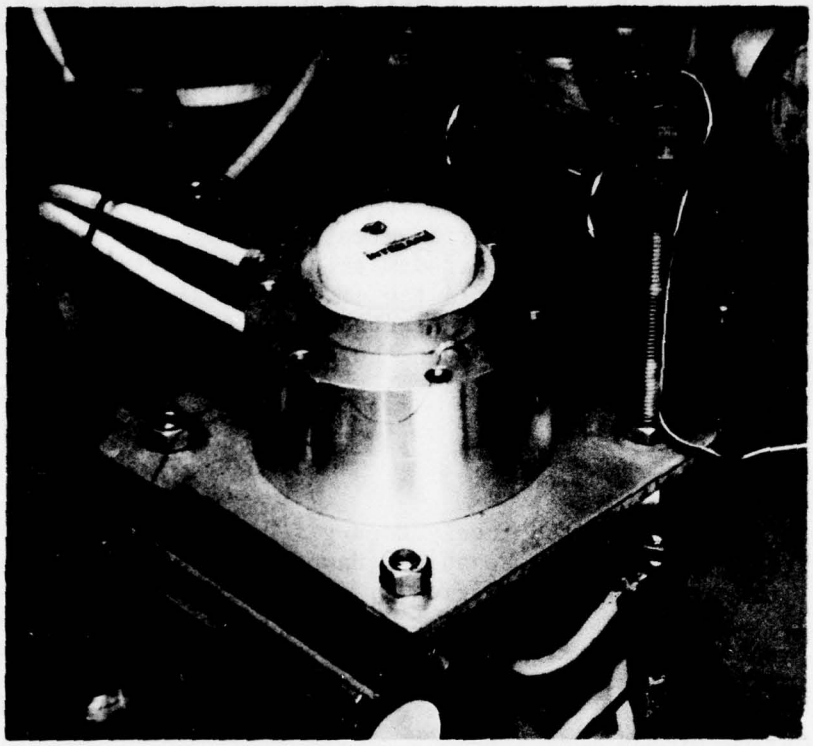

Figure 1. Gas-Bearing Suspension System

DISPLACEMENT MEASUREMENT

The measurement system is based on an instrument called the Fotonic Sensor, manufactured by Mechanical Technology, Inc. The light-probe assembly can be seen behind the ring in figure 1, and the displacement measurement apparatus is shown completely in figure 2. The probe, diagramed in figure 3, is composed of two bundles of optical fibers -- one to transmit light to a reflecting surface, and the other to return reflected light to a photodetector. The fibers at the end of the probe are randomly distributed inside a metallic cylinder approximately 3.0 in. (76.2 mm) long by 0.125 in. (3.18 mm) in diameter. The face of the cylinder containing the random distribution of fibers is positioned (by means of a rack and pinion mount) near the surface to be measured, and the separation between the face of the probe and the surface is determined with a calibrated dial indicator (see figure 5). Thus, measurements can be made without contacting or mechanically loading the object.

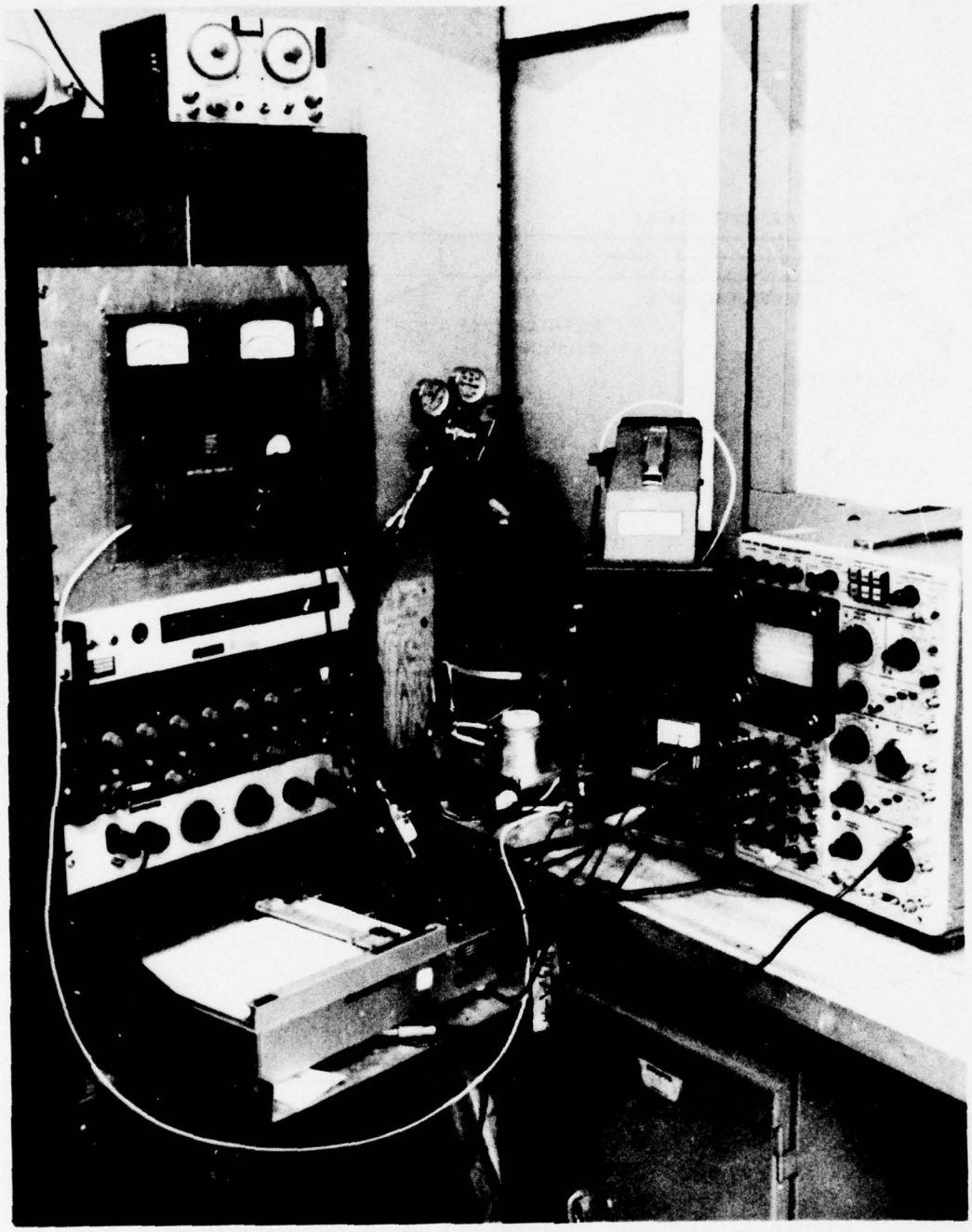

Figure 2. Complete Measurement System

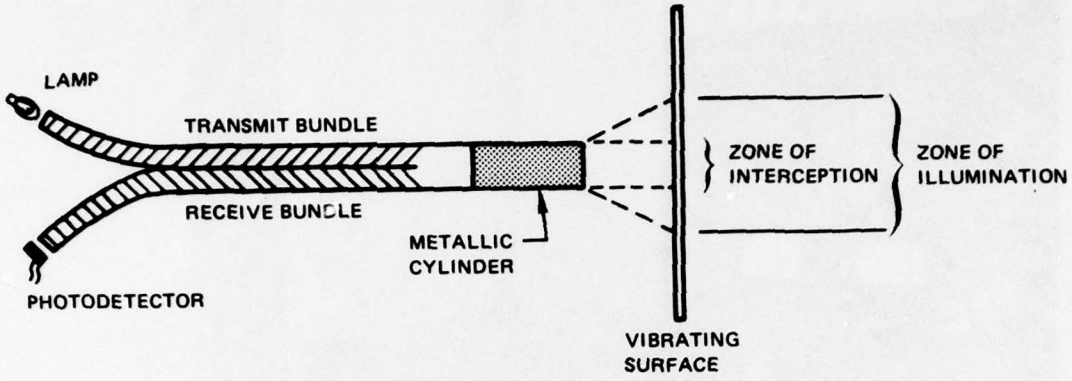

Figure 3. Diagram of Light-Probe Assembly

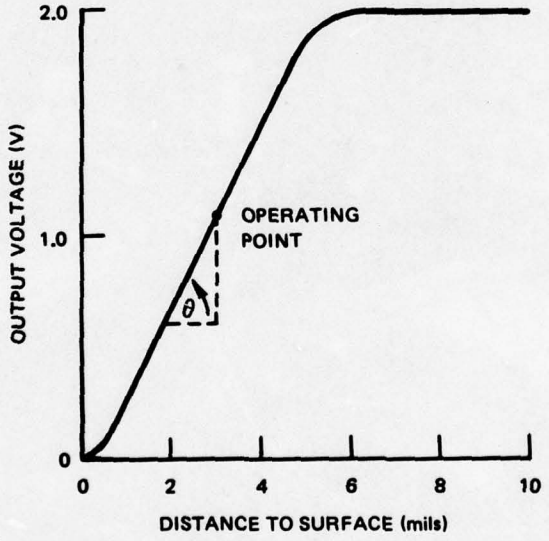

Figure 4. Typical Calibration Curve for Fotonic Sensor (sensitivity (mV/nm) = tan θ ; 1 mil = 25.4μm)

Calibration of the instrument is done statically, and a typical curve is shown in figure 4. A large linear region of operation is available, and for vibration measurements the distance of the optical probe from the surface of the object is approximately the center of this linear region. The slope of the calibration curve is the dynamic sensitivity of the instrument and is dependent on the reflectivity of the surface of the object. Because the ceramic itself is not a good reflector, a small polished copper tab was placed on the outside cylindrical surface of each ring to enhance the dynamic sensitivity.

The particular model of sensor used in these measurements had a flat frequency response from dc to 100 kHz. Figure 5 is a diagram of the ceramic ring, the gas-bearing assembly, and the displacement measurement equipment.

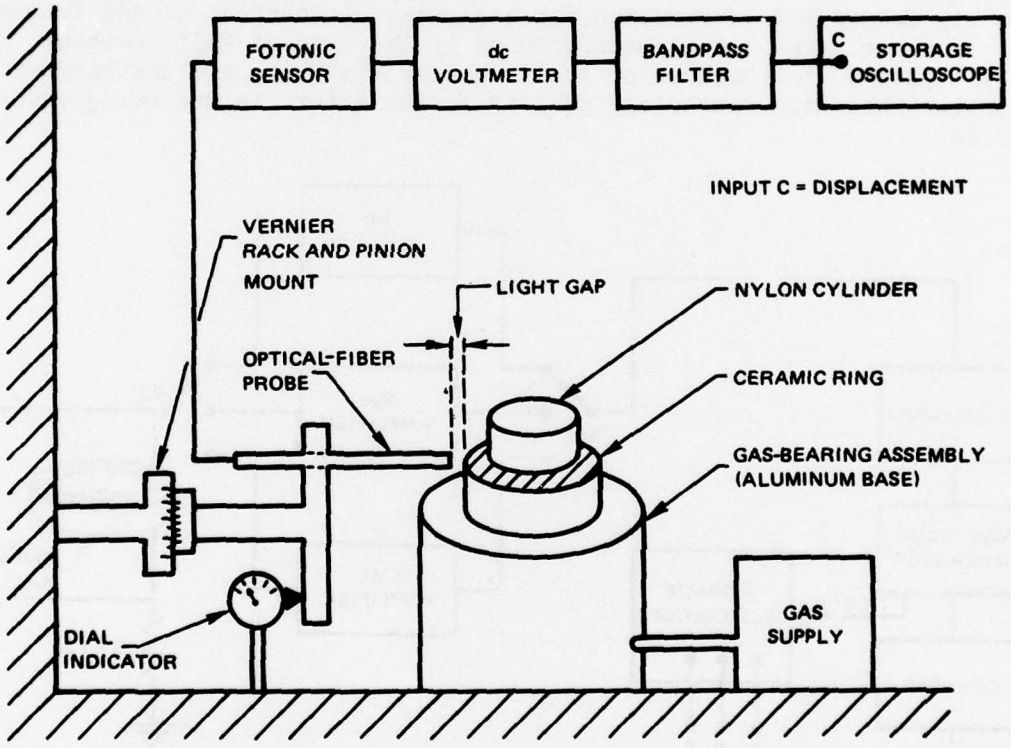

Figure 5. Block Diagram of Dynamic-Displacement Measurement Apparatus

ELECTRICAL DRIVING SYSTEM

Figure 2 shows the complete measurement system. The large unit in the top of the rack is a complex impedance-admittance meter (CIAM) manufactured by Dranetz Engineering Laboratories, Inc.; it is used to measure the low-level linear parameters of the ceramic test specimens. This unit operates with a constant continuous wave (CW) signal amplitude of 3.0 Vrms across the ceramic. Low-level pulse measurements at the same voltage are compared with the CW measurements to ensure that the pulse system is operating properly. Figure 6 is a block diagram of the electrical driving system, which utilizes three separate power amplifiers in order to provide clean electrical driving signals from low level to high level (fracture). A sinusoidal driving voltage of short duration (pulsed signal) is used to keep heating effects in the ceramic to a minimum, especially at high levels. A Tektronix 549 storage oscilloscope retains the voltage, current, and displacement pulse envelopes and the expanded waveforms, and a Polaroid oscilloscope camera is used to permanently record the information for analysis. A coherent decade frequency synthesizer, type 1161-A manufactured by the General Radio Company, is the signal source because of its frequency stability and low harmonic content when high mechanical quality factor materials are being investigated.

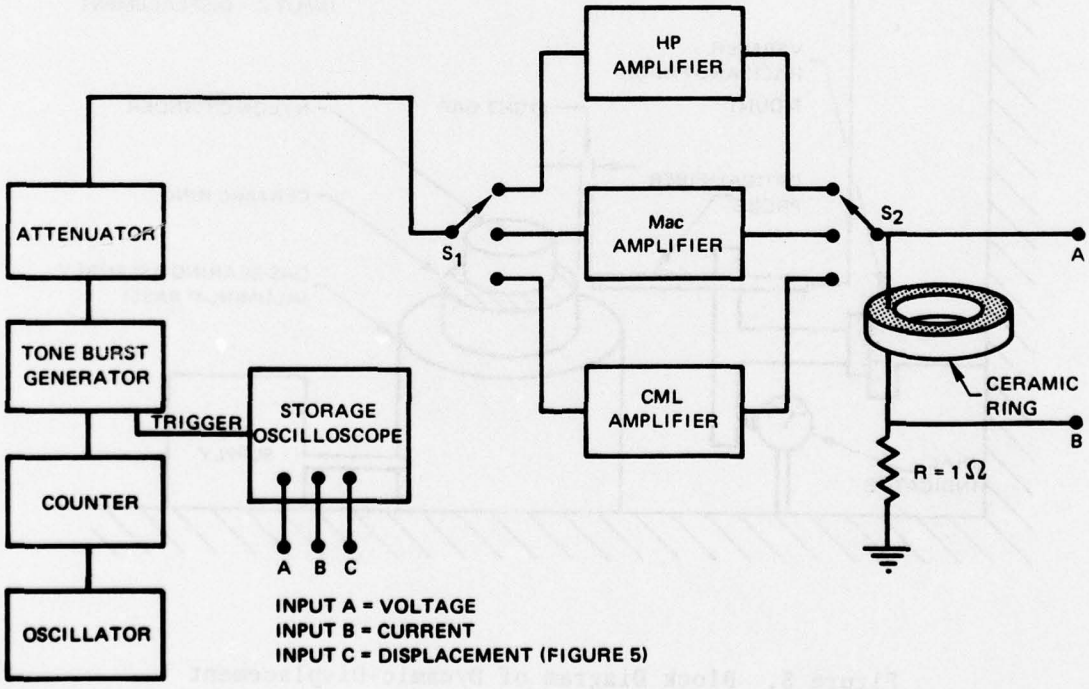

Figure 6. Block Diagram of Electrical Driving System

REPRESENTATIVE DATA

Some of the basic types of information available with the present measurement setup are illustrated in figure 7. Figure 7a shows (from top to bottom) the profiles of voltage, current, and displacement pulses for a trial run at low drive level -- approximately 3.5 V, or 7 x 10^{-3} V/mil (0.28 kV/m) across a 0.50 in. (12.7 mm) ceramic specimen. The time scale on the horizontal sweep of the oscilloscope is 20 msec per division, and the voltage pulse length shown is approximately 80 msec. Close scrutiny of the lower displacement trace indicates that steady-state conditions exist over the range from 50 to 80 msec. In other words, a minimum driving pulse length of 50 msec is required for the ring to reach steady-state conditions, and driving it with a voltage pulse less than 50 msec long will not yield information indicative of steady-state material parameters, -- which is one goal of this investigation.

Figure 7b shows an expanded view of the current decay after voltage cutoff; the current was determined from the voltage drop across a 1-Ω resistor in series with the ring impedance at resonance (see figure 6; the impedance of the ring is roughly 100 times greater than that of the 1-Ω series resistor), from which the mechanical quality factor Q_M of the ring was obtained. The current decay, which is indicative of the mechanical losses in the ceramic, is not strictly exponential at high drive levels (as is common in linear systems) and offers the greatest potential for measurement error and misinterpretation in the overall setup. Gerson[10] employed a resistance substitution method to demonstrate to some extent that Q_M decreased with increasing stress level and that the stress level depended on the electrical drive level. Therefore, when the voltage is abruptly shut off at the end of the pulse, the stresses in the ring continuously decrease, causing the so-called quality factor* to apparently increase with time of decay. Although a more detailed discussion of this specific problem will follow, let it suffice at this point to say that the decay of the current after voltage shutoff in a steady-state condition is normally used as a measure of the losses in a linearly responsive system.

---

*Quality factor is defined in electrical engineering terminology for linear systems only and, as such, is undefined when nonlinear phenomena exist.

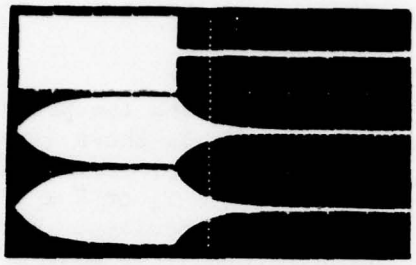

7a. Voltage, current and displacement envelopes

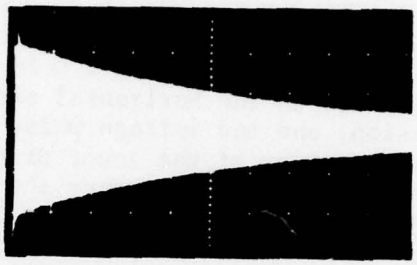

7b. Current decay

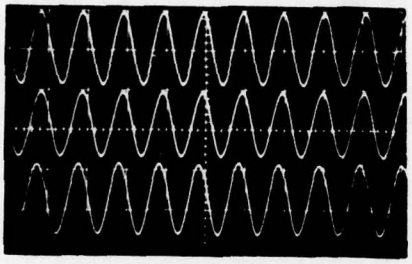

7c. Voltage, current, and displacement steady-states

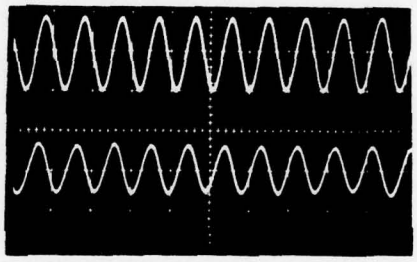

7d. Voltage and current at 1 kHz

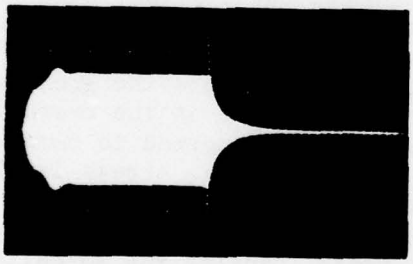

7e. Current at f_o = 18.4520 kHz

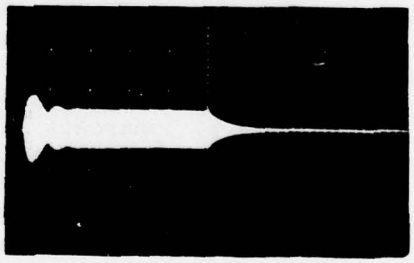

7f. Current at f_ℓ = 18.4421 kHz

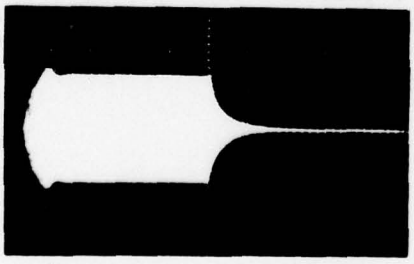

7g. Current at f_u = 18.4621 kHz

Figure 7. Representative Data Waveforms

Figure 7c shows the steady-state magnitudes of all three quantities (voltage, current, and displacement) at resonance of the ring by time-delaying a 50 μsec/cm portion of the steady-state region of the pulse envelope. These magnitudes are used to plot current and strain values, as well as stress levels, versus electric driving fields, irrespective of phase relationships.

Figure 7d depicts the magnitudes of the voltage and current at 1 kHz, a frequency that is well below resonance of the ring (which occurs at approximately 18.64 kHz) in order to ensure being in the stiffness-controlled frequency region to obtain capacitance values at discrete drive levels. This measurement yields the variation of the permittivity with drive level and can be used to correct the calculated stress level in the ring.

Additional information of the type shown in figures 7e, 7f, and 7g is also available. The figures are traces, with the same vertical scaling previously used, of the current through an Edo Western ceramic ring at a driving field of 0.1 V/mil (3.93 kV/m). Figure 7e is the current at the resonance frequency f_o and shows that the initial current response to this field level does not have the same uniform characteristics as the response at low level (see figure 7a); the resonance frequency has also decreased about 150 Hz from the initial low-level value (18.6 kHz) for this ring. Figures 7f and 7g show the current responses at frequencies f_l and f_u, 10 Hz below and above resonance, respectively. These traces demonstrate the highly nonlinear behavior of Type-I ceramic at large vibration amplitudes inasmuch as the response is not symmetrical in the frequency domain about resonance. As the amplitude is increased further, jump phenomena, characteristic of a nonlinear oscillator,[11] occur, as demonstrated by Negishi.[3] The mechanical displacement amplitude of the ring exhibits the same phenomenon.

Figure 8 illustrates the benefits of filtering. The top trace in figure 8a is the output of the Fotonic sensor and shows the low frequency distortion caused by erratic motion of the electrical leads attached to the ring and of the ring itself on the gas bearing. The bottom trace is the same output after filtering through a 2600 Hz to 50 kHz bandpass filter; figure 8b is an expanded view of the steady-state signal and shows the amount of attenuation introduced by the filter.

EXPERIMENTAL DATA AND INTERPRETATIONS

Several rings were driven electrically to dynamic fracture, but only two rings (Edo Western ring number 001 and Channel Industries ring number 23, henceforth referred to as ring A and ring B, respectively) were measured sufficiently to provide reliable data.

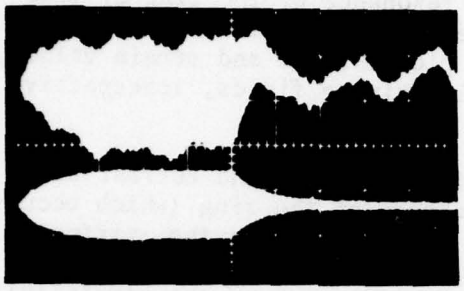

8a. Unfiltered and filtered envelopes

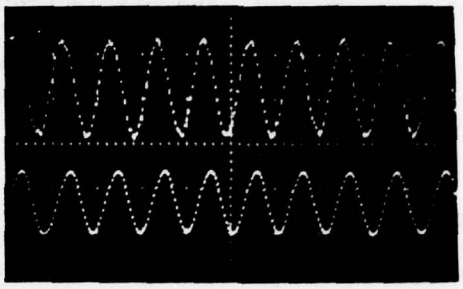

8b. Unfiltered and filtered steady-states

Figure 8. Fotonic Sensor Output Waveforms

The measurements were recorded under pulsed electrical drive with the rings mounted on the gas-bearing suspension system. Initially, low-level pulse measurements were made, and the results were compared with continuous wave measurements made at the same drive level in order to ensure that the pulse measurement system was operating properly. Differences in the resonance frequencies for the two methods were less than 0.1 percent, and the values of Q_M determined from the electrical admittance plot and from the current decay were within 2 percent of each other. This latter result gave credence to the technique of determining Q_M from the current decay. The measured mechanical displacement of ring A was within 10 percent of the value predicted from the low-level linear parameters for that specimen and verified the calibration of the displacement probe.

SUSPENSION-SYSTEM LOSS

During this low-drive-level phase of the investigation it was discovered that the gas-bearing suspension system introduced unaccountable mechanical losses. This problem is evidenced by figure 9, which shows two complex admittance plots of ring B -- one with the ring freely suspended from a rubber band, and the other with the ring mounted on the gas bearing. Under the low-level linear drive conditions used for the measurements, Q_M is defined as

$$Q_M = \frac{\omega_r^E M}{R_M} = \frac{f_r^E}{f_2 - f_1}, \qquad (1)$$

where

$\omega_r^E = 2\pi f_r^E$,

f_r^E is the resonance frequency at constant electric field E,

M is the mass of the ceramic ring (M = ρ V, where ρ is the density of the material and V is the volume of the ring),

R_M is the mechanical loss associated with the ring material, and

f_1, f_2 are the quadrantal or half-power frequencies.

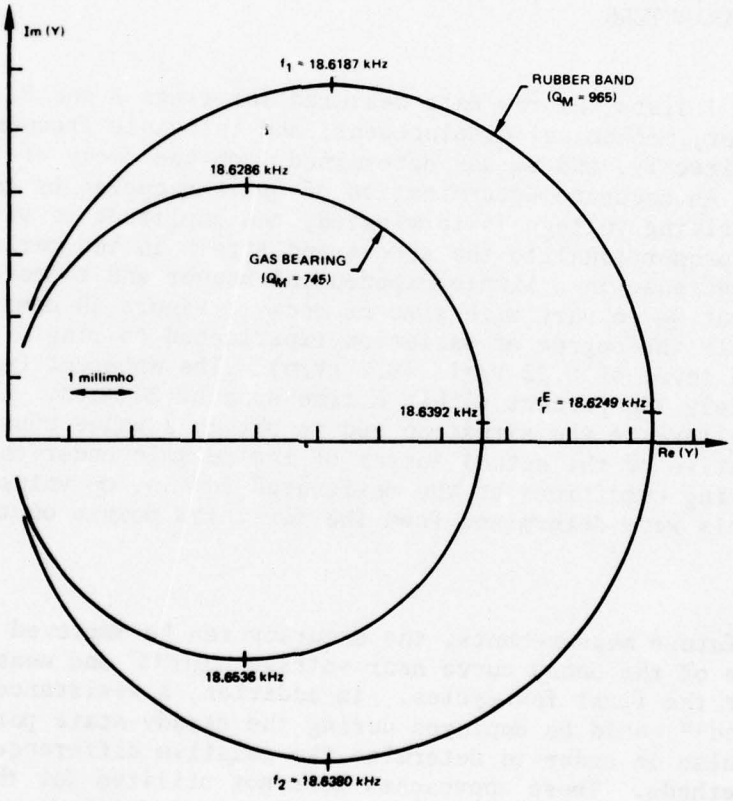

Figure 9. Complex Admittance Plots for Hard Lead-Zirconate-Titanate Ceramic Ring (f_r^E is hoop-mode resonance frequency; f_1 and f_2 are quadrantal frequencies)

When the ring was mounted on the gas bearing, the value for Q_M decreased 23 percent (that is, the electromechanical resistance increased from 97.5 Ω to 130.7 Ω), and the resonance frequency increased about 15 Hz. These anomalies are probably due to the fact that there is a confined air space between the inside wall of the ring and the nylon center support of the gas bearing that introduces acoustic stiffness and loss. Improvements in the design of the gas bearing should alleviate such problems. Inasmuch as there was no apparent correction factor that would account for the additional loss and inasmuch as the gas-bearing suspension was still needed to make displacement measurements on the rings, all variations in parameters at higher levels were compared with low-level values measured with the rings mounted on the same gas bearing.

OBSERVED PARAMETERS

Table 1 lists the raw data measured for rings A and B. The voltage, current, mechanical displacement, and resonance frequency were measured directly, and Q_M was determined from the decay of the current envelope. An accurate determination of Q_M is hampered by the fact that once the driving voltage is terminated, the amplitude of vibration (which is proportional to the stress and strain in the ceramic ring) does not decrease in a simple exponential manner and therefore causes the apparent Q_M to vary with time of decay. *Figure 10 demonstrates* emphatically the degree of variation experienced on ring A at an electric field level of 0.22 V/mil (8.7 kV/m). The apparent Q_M increased approximately 180 percent within a time span of 20 msec. Therefore, in order to alleviate the situation and to obtain a value considered to be representative of the actual losses of the ceramic under the steady-state driving conditions at the designated levels, Q_M values for all drive levels were determined from the first few points on the decay curve.

For future measurements, the accuracy can be improved by expanding the region of the decay curve near voltage cutoff and measuring the decay over the first few cycles. In addition, a resistance substitution method[10] could be employed during the steady-state portion of the driving pulse in order to determine the relative differences between the two methods. These approaches were not utilized for this series of measurements because the variation problem in Q_M with decay at high drive level was not recognized until after the measurements had been completed (and the samples had fractured).

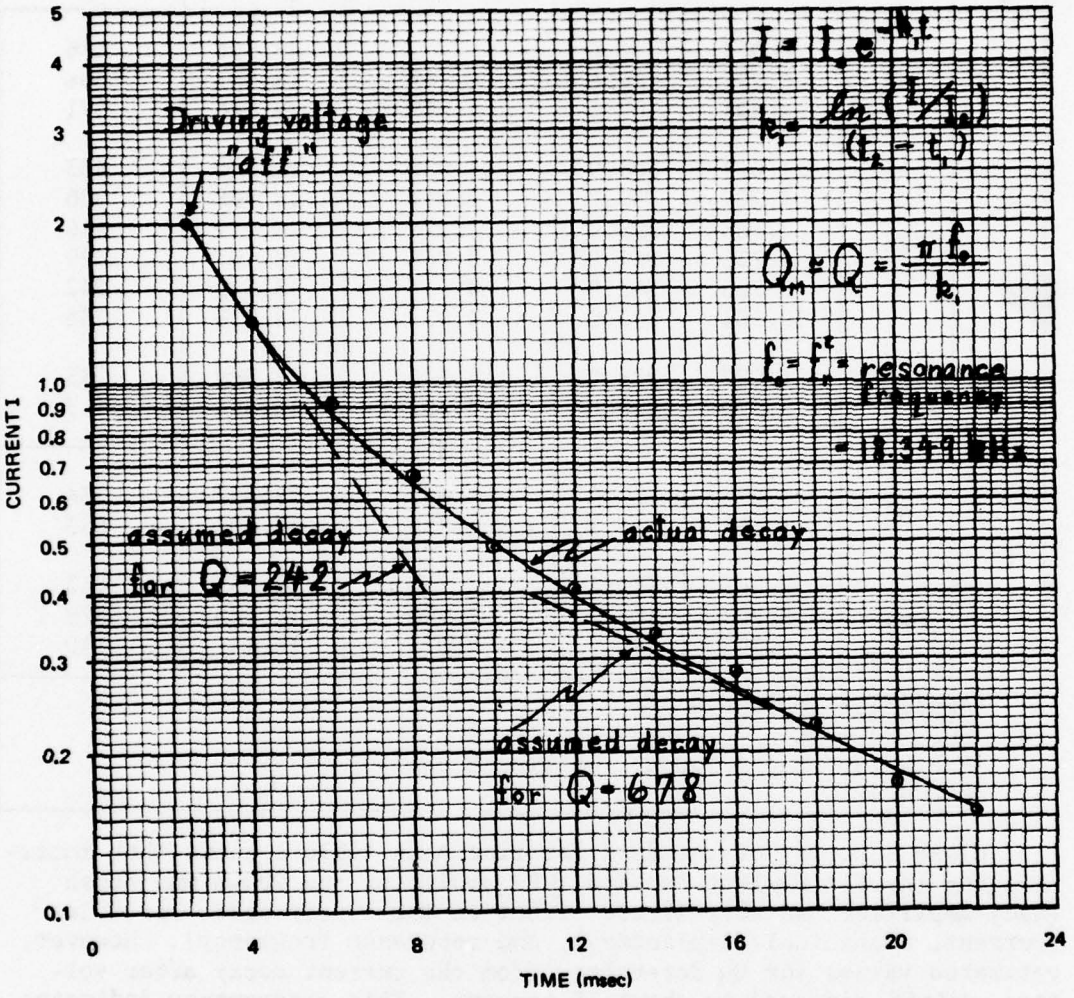

Figure 10. Top Half of Current Decay Envelope

Table 1. Measured Data for Ceramic Rings

Ring	Amplifier*	Electric Field E_3 (kV/m)	Current I (mA)	Mechanical Displacement $u_{r=b}$ (μm)	Resonance Frequency f_r^E (kHz)	Mechanical Quality Factor Q_M
A	HP	0.027	3.6	--	18.598	686
		0.272	40.6	0.748	18.591	696
		1.091	107.5	1.973	18.546	571
	Mac	1.091	108.9	1.958	18.543	483
		2.227	159.0	2.814	18.498	526
		3.786	198.0	3.278	18.452	416
		6.235	247.0	3.945	18.407	329
		8.795	282.8	4.917	18.349	242
		10.354	293.0	4.931	18.313	236
	CML	11.022	235.0	4.329	18.399	185
		12.526	239.0	4.337	18.374	167
B	HP	0.273	29.9	0.601	18.637	734
		1.135	93.3	1.880	18.604	653
	Mac	2.547	129.4	3.256	18.555	543
		5.761	173.2	3.950	18.483	479
		9.297	180.3	4.071	18.427	140

*Amplifier Impedance
HP - < 1 mΩ
Mac - for ring A 100 Ω, for ring B 66 Ω
CML - 64 Ω

Close scrutiny of the data for ring A in table 1 shows that interchanging the 5-W Hewlett-Packard (HP) amplifier and 200-W MacIntosh (Mac) amplifier had very little effect on the steady-state variables (current, mechanical displacement, and resonance frequency). However, estimated values for Q_M determined from the current decay after voltage cutoff differed by about 15 percent. This discrepancy indicates that another potential problem in determining Q_M values from current decay information exists because of the influence of the amplifier impedance, which becomes part of the decay circuit during the off-time of the driving pulse. This particular type of problem may be circumvented by using the previously mentioned substitution method -- namely, inserting an appropriate resistance for the ceramic ring in order to obtain an equivalent input current value at the same driving (resonance) frequency and drive level, and then computing the variation in

the quality factor in terms of the low-level value ($Q_M = \omega_r^E M / R_M$), assuming the mass reactance term to be essentially constant and the blocked impedance of the ring to be much larger than the mechanical resistance at resonance. Appendix A gives a brief description of the influence of the amplifier impedance on the quality factor in a simplified electrical circuit and demonstrates the need for considering such a potential problem with current-decay type measurements.

The apparent decrease in the current and displacement of ring A when the 5-kVA Communications Measurement Laboratory (CML) amplifier was used was not due to the amplifier itself but, rather, to a thin sheet of cellophane that was placed between the lower electrode of the ring near the electrical lead and the grounded aluminum housing of the gas suspension system in order to prevent arcing at the higher drive levels. The cellophane added a small amount of stiffness that resulted in an increase in the resonance frequency. The effect of the cellophane on the measured data was taken into account by extending the curves in the region of saturation -- as demonstrated in figure 11, which is a plot of the steady-state strain S_b, determined from the measured displacement $u_{r=b}$ (where b is the outside radius of the ring) and input current I, versus the electric field, all in rms values. The last points on the graph (at $E \simeq 14$ kV/m) correspond approximately to the field level at which ring A fractured. The values for S_b and I at this field level are not included in table 1 because of the bizarre behavior of the strain value, which was attributed to faulty positioning of the displacement probe. It should be noted, however, that the last three points for the current track well and appear to have a linear relationship. Therefore, the strain value at fracture is estimated from the extended strain curve at the critical field to have a value $S_b = 159 \times 10^{-6}$ m/m. This value was used to determine the stress level at which fracture occurred.

LINEAR INTERPRETATION

Inasmuch as there is presently no precise nonlinear mathematical theory for predicting the high-strain behavior of ceramics at sonic frequencies, the experimental data presented in this report are interpreted solely in terms of the variation of the low-level, linear ceramic parameters as a function of state variables (electric field, stress, etc.). The definitions given to the low-level parameters (or combinations of parameters) are determined from linear theory, starting with the linear equations of state for a mechanical one-dimensional vibrator. For the rings under consideration in this investigation, for instance,

$$S_1 = s_{11}^E T_1 + d_{31} E_3 \quad \text{and} \tag{2a}$$

$$D_3 = d'_{31} T_1 + \varepsilon^T_{33} E_3 \qquad (2b)$$

relate strain S_1 and electric displacement D_3 to stress T_1 and electric field E_3, where

s^E_{11} is the compliance coefficient at constant electric field ($E_1 = E_2 = 0$),

ε^T_{33} is the permittivity at constant stress ($T_2 = T_3 = 0$), and

d_{31}, d'_{31} are piezoelectric coefficients.

The coefficients, which are constants in the linear case, are allowed to become level-dependent when the above equations are applied to the large-signal case (nonrigorous mathematical approach). Reciprocity should not be assumed when nonlinear effects are present; therefore, the prime on d_{31} in equation (2b) indicates that it may have a value different from d_{31} in equation (2a).

The dynamic equations for the ring are obtained by combining the equations of state with the expression for the stress due to inertia

$$T_1 = \rho \omega^2 r_m^2 S_1 , \qquad (3)$$

where

r_m is the mean radius of the ring,

ρ is its density, and

ω is the angular frequency.

Substituting equation (3) into equation (2a) yields an expression for the dynamic strain --

$$S_1 = \frac{d_{31} E_3}{\left[1 - \omega^2 r_m^2 \rho s^E_{11}\right]} . \qquad (4)$$

In reality, the compliance coefficient is complex,

$$s_{11}^{E} = s_{11}^{E'} - js_{11}^{E''} \quad ,$$

and its components are utilized in the expressions for the resonance frequency

$$\omega_r^E = \left(r_m^{\,2} \, \rho s_{11}^{E'} \right)^{-1/2} , \tag{5}$$

and the mechanical quality factor at resonance,

$$Q_M = s_{11}^{E'} \Big/ s_{11}^{E''} \quad .$$

In terms of these parameters the dynamic strain becomes

$$S_1 = S_m = \frac{d_{31} E_3}{\left[1 - \left(\frac{\omega}{\omega_r^E} \right)^2 \left(1 - \frac{j}{Q_M} \right) \right]} \tag{6}$$

or

$$S_m = -jd_{31} Q_M E_3 \text{ at } \omega = \omega_r^E \, , \tag{7}$$

where S_m is the mean strain in the ring defined as $S_m = u_{r=r_m} \Big/ r_m$.

The input current to the ceramic ring may also be determined by manipulation of equation (2a) into equation (2b) such that

$$D_3 = \frac{I}{j\omega A} = d_{31}' \left(\frac{1}{s_{11}^E} S_1 - \frac{d_{31}}{s_{11}^E} E_3 \right) + \varepsilon_{33}^T E_3 \tag{8}$$

since $q = \int D_3 dA$ and $I = dq/dt = j\omega q$, where q is the total electrical charge and A is the electrode area of the ceramic ring. Rearrangement of equation (8) in conjunction with equation (6) yields

$$\frac{I}{j\omega A} = \frac{\dfrac{d_{31}d'_{31}}{s^E_{11}}}{\left[1 - \left(\dfrac{\omega}{\omega^E_r}\right)^2\left(1 - \dfrac{j}{Q_M}\right)\right]} E_3 + \epsilon^T_{33}\left(1 - \frac{d_{31}d'_{31}}{\epsilon^T_{33}s^E_{11}}\right)E_3. \qquad (9)$$

At resonance, $\omega = \omega^E_r$, equation (9) reduces to

$$I = \frac{\omega^E_r A Q_M d_{31} d'_{31}}{s^E_{11}} E_3, \qquad (10)$$

which is simply the motional component of the total input current under the assumption that the blocked component of the current is negligible (that is,

$$\omega^E_r A \epsilon^T_{33}\left(1 - \frac{d_{31}d'_{31}}{\epsilon^T_{33}s^E_{11}}\right)E_3 \ll \frac{\omega^E_r A Q_M d_{31} d'_{31}}{s^E_{11}} E_3;$$

see appendix B).

It is apparent, then, that figure 11 is simply a plot of the magnitudes of equations (7) and (10) at resonance of the ring, with the mean strain values replaced by the strain values at the outside radius of the ring because these latter values were more directly related to the actual measurements. The relationship between the strain at r = b and the mean strain at $r = r_m$ is given[12] as

$$\frac{S_m}{S_b} = \frac{b}{r_m}\frac{u_{r=r_m}}{u_{r=b}} = \frac{b}{r_m}\frac{1}{\left[1 + \sigma^E\left(1 - \dfrac{b}{r_m}\right)\right]} = 1.153, \qquad (11)$$

where σ^E is Poisson's ratio for the ceramic material at constant electric field and has been given the value of 0.33 for this exercise.

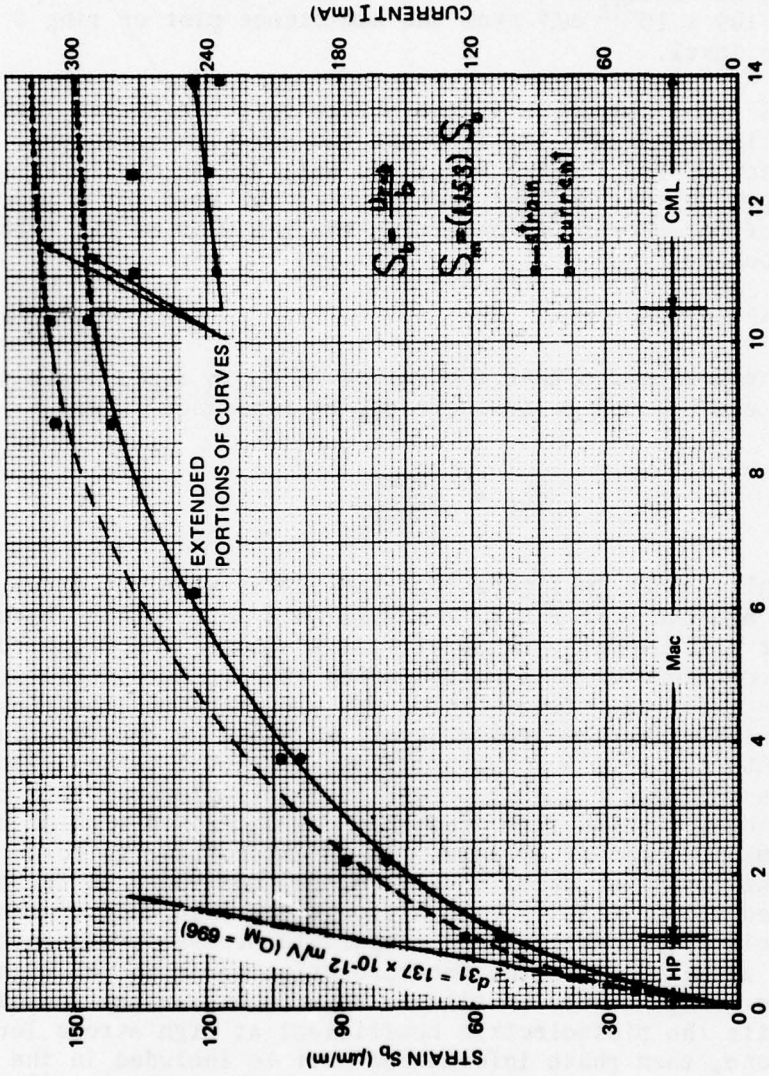

Figure 11. Steady-State Strain and Current versus Electric Field for Ring A

The linear low-level piezoelectric coefficient d_{31} was determined from the graph (based on a value of Q_M = 696 (E = 0.272 kV/m)) to be 137 x 10^{-12} m/V, which compares well with the value 130 x 10^{-12} m/V calculated from the low-level admittance plot of ring A. Figure 12 is a similar type of plot for ring B; the linear piezoelectric coefficient for this case was determined to be d_{31} = 118 x 10^{-12} m/V, compared with the value of 109 x 10^{-12} m/V from the admittance plot of ring B at a similar drive level.

Figure 13 is a composite of the strain versus electric field curves from figures 11 and 12; it shows the relative difference in strain at fracture for the two rings, as well as the nonlinear variation of the product d_{31} Q_M, and demonstrates the need for a precise measurement of Q_M in order to determine the behavior of d_{31} with drive level at resonance.

CALCULATED PARAMETERS

Under the assumption that the values of Q_M in table 1 are valid, equation (7) can be used to evaluate d_{31} at resonance, where

$$d_{31} = \frac{|Sm|}{|Q_M E_3|} , \tag{12}$$

with the results shown in figure 14. The curves were not drawn point to point but are the best fit to the available data points (haphazard at the higher drive levels, especially at fracture) and might not represent the true behavior of d_{31} with drive level. Nevertheless, there appears to be a definite tendency for the piezoelectric coefficient to decrease with the increased drive level, as shown by the departure of the data points for ring A from the linear low-level value. The same comment holds for ring B. This result is in disagreement with previous observations,[13] which indicated that d_{31} increased with ac drive level for similar types of ceramic. It is interesting to note, however, that the low-level dynamic value of d_{31} was found to decrease[14] with increased static bias stress, although the magnitude of the decrease was relatively small at the comparable stress levels encountered here. It may be that the interpretation given to the high-level dynamic value of d_{31} should be altered to account for any losses[15] associated with the piezoelectric coefficient at high stress levels. If this is done, then phase information must be included in the measurement program. Nevertheless, the data presented by Gerson[10] were based on the assumption that d_{31} remained constant with stress level (this particular point will be discussed in more detail).

Clarification of these discrepancies can only be achieved by more detailed measurements on additional ceramic specimens.

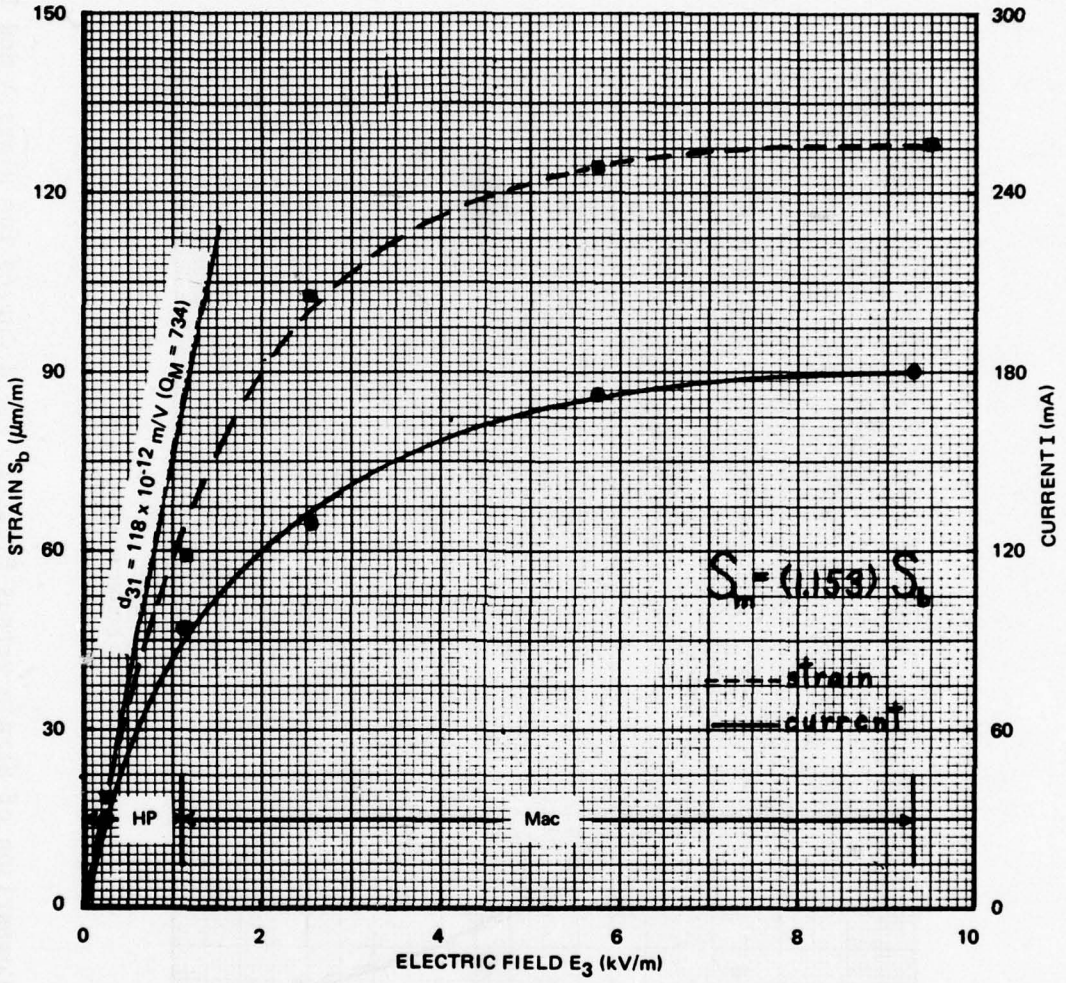

Figure 12. Steady-State Strain and Current versus Electric Field for Ring B

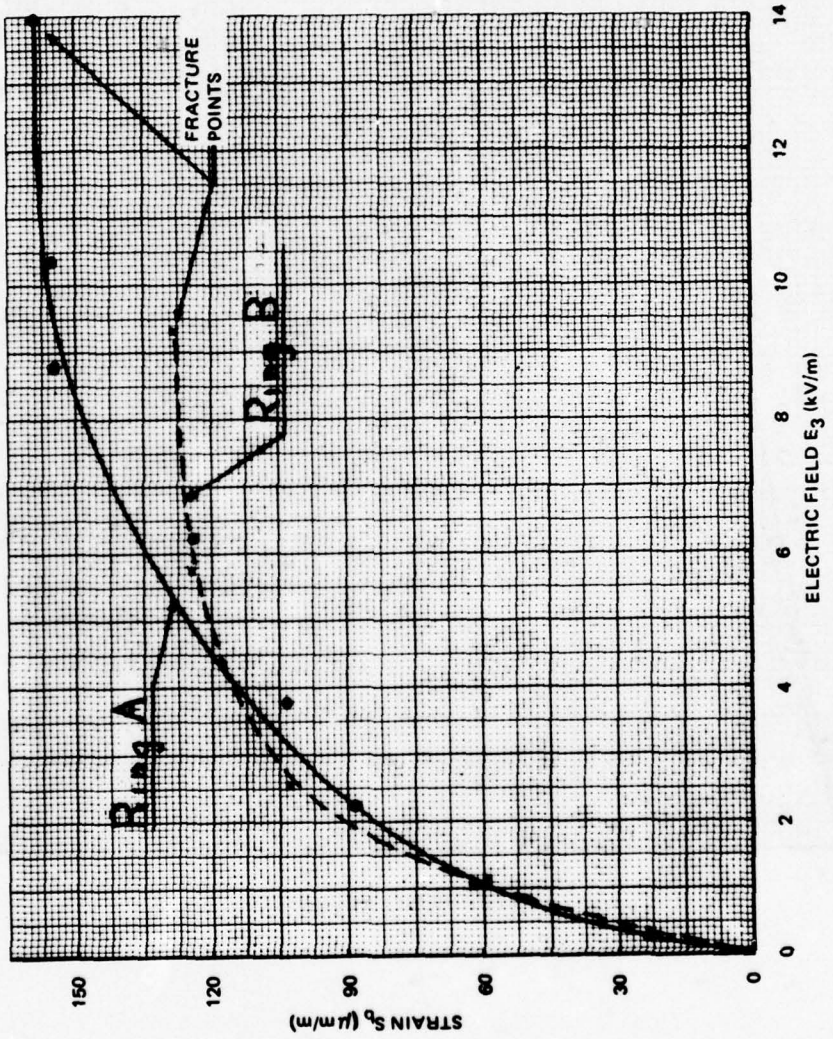

Figure 13. Comparison of Strain versus Electric Field Curves for Rings A and B

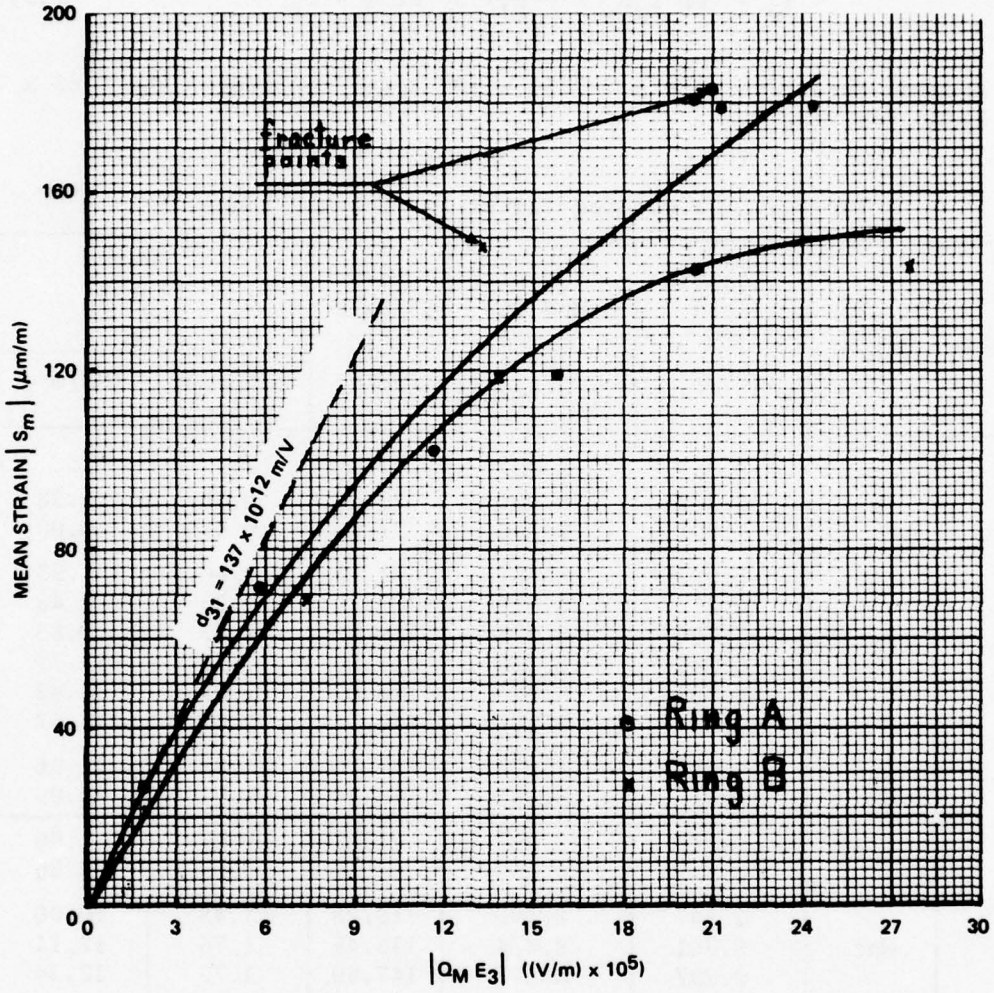

Figure 14. Behavior of Piezoelectric Strain Coefficient d_{31}

Values for the mean strain S_m and Young's modulus $1/s_{11}^{E'}$ were calculated for each electric field point in table 1 by using equations (11) and (5), and the resulting data are listed in table 2 along with the mean stress

$$T_m = \rho\omega^2 r_m^2 S_m = \frac{1}{s_{11}^{E'}} S_m \text{ at } \omega = \omega_r^E \quad . \tag{13}$$

The assumed densities were $\rho = 7.54 \times 10^3$ kg/m^3 for ring A and 7.65×10^3 kg/m^3 for ring B.

Table 2. Calculated Values for Ceramic Rings

Ring	Amplifier*	Electric Field E_3 (kV/m)	Young's Modulus $1/s_{11}^{E'}$ (10^{10}N/m^2)	Mean Strain S_m (μm/m)	Mean Stress T_m	
					(lbf/in.^{2} × 10^3)	(MN/m^2)
A	HP	0.027	8.407	---	---	---
		0.272	8.401	27.18	0.33	2.28
		1.091	8.360	71.66	0.87	6.00
	Mac	1.091	8.357	71.13	0.86	5.93
		2.227	8.317	102.21	1.23	8.48
		3.786	8.275	119.08	1.43	9.86
		6.235	8.235	143.30	1.71	11.79
		8.795	8.183	178.62	2.12	14.62
		10.354	8.151	179.14	2.12	14.62
	CML	11.022	8.228	157.26	1.88	12.96
		12.526	8.206	157.54	1.87	12.89
B	HP	0.273	8.565	21.83	0.27	1.86
		1.135	8.535	68.30	0.85	5.86
	Mac	2.547	8.490	118.28	1.45	10.00
		5.761	8.424	143.48	1.76	12.14
		9.297	8.373	147.89	1.79	12.34

*Amplifier Impedance
HP - < 1 mΩ
Mac - for ring A 100 Ω, for ring B 66 Ω
CML - 64 Ω

The mechanical quality factor Q_M, the proportional decrease in Young's modulus ($Y_{11}^E = 1/s_{11}^E$), and the proportional decrease in the piezoelectric strain coefficient d_{31} are plotted versus the mean stress (rms) values in figures 15 and 16 for rings A and B. Here Q_M and $1/s_{11}^E$ follow the same general trend of variation as Gerson's measurements, and the magnitudes of the decreases for these quantities are strikingly similar to his results if aging of the rings is allowed for and the stress values quoted in this report are converted to peak values. Gerson's observations that the Q_M values increase with aging and that the variation with stress level becomes more linear* are confirmed by the NUSC measurements. Gerson also found that the variation in Young's modulus with drive level was less severe for well-aged ceramic specimens, and this is confirmed by the measurement data presented in this report. Minor differences in values, as measured by Gerson or at NUSC, can be attributed to differences in the ceramic sample properties, which are outlined in table 3 for comparison.

Table 3. Properties of Ceramic Samples

Ceramic Property	Gerson[10]†	NUSC‡	
		Ring A	Ring B
k_{31}	0.247	0.355	0.326
K_{33}^T(1kHz)	1240	1278	1077
d_{31}	-92×10^{-12} m/V	-130×10^{-12} m/V	-109×10^{-12} m/V
Y_{11}^E	7.92×10^{10} N/m^2	8.39×10^{10} N/m^2	8.57×10^{10} N/m^2
Q_M	530	833	965

†$Pb_{0.94}\ Sr_{0.06}\ Zr_{0.53}\ Ti_{0.47}\ O_3$ ceramic, radially poled rings, suspended by thread, and measured 200 days after poling.
‡Navy Type-I ceramic, axially poled rings, suspended by rubber band, and measured 3 years after poling.

*The plots of Q_M versus peak dynamic stress in Physical Acoustics[1] (p. 217) are apparently for newly poled ceramics inasmuch as the initial slope of the curves is quite steep.

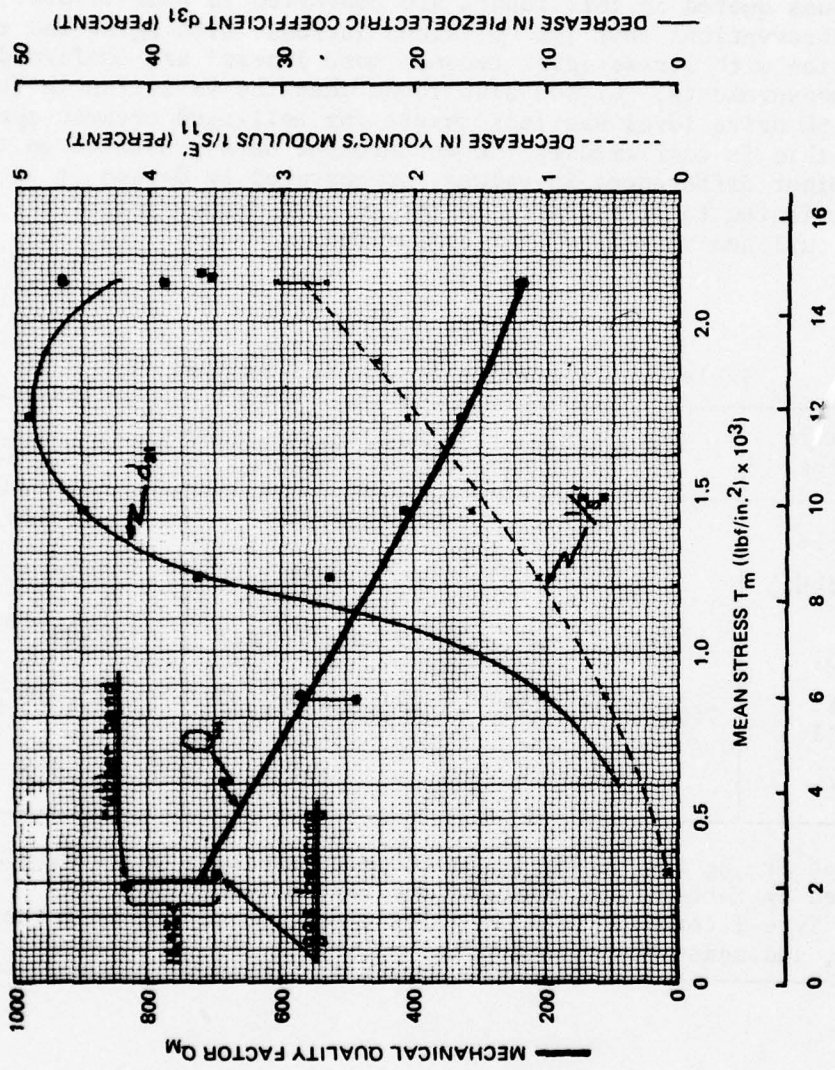

Figure 15. Mechanical Quality Factor, Decrease in Young's Modulus, and Decrease in Piezoelectric Coefficient versus Mean Stress for Ring A

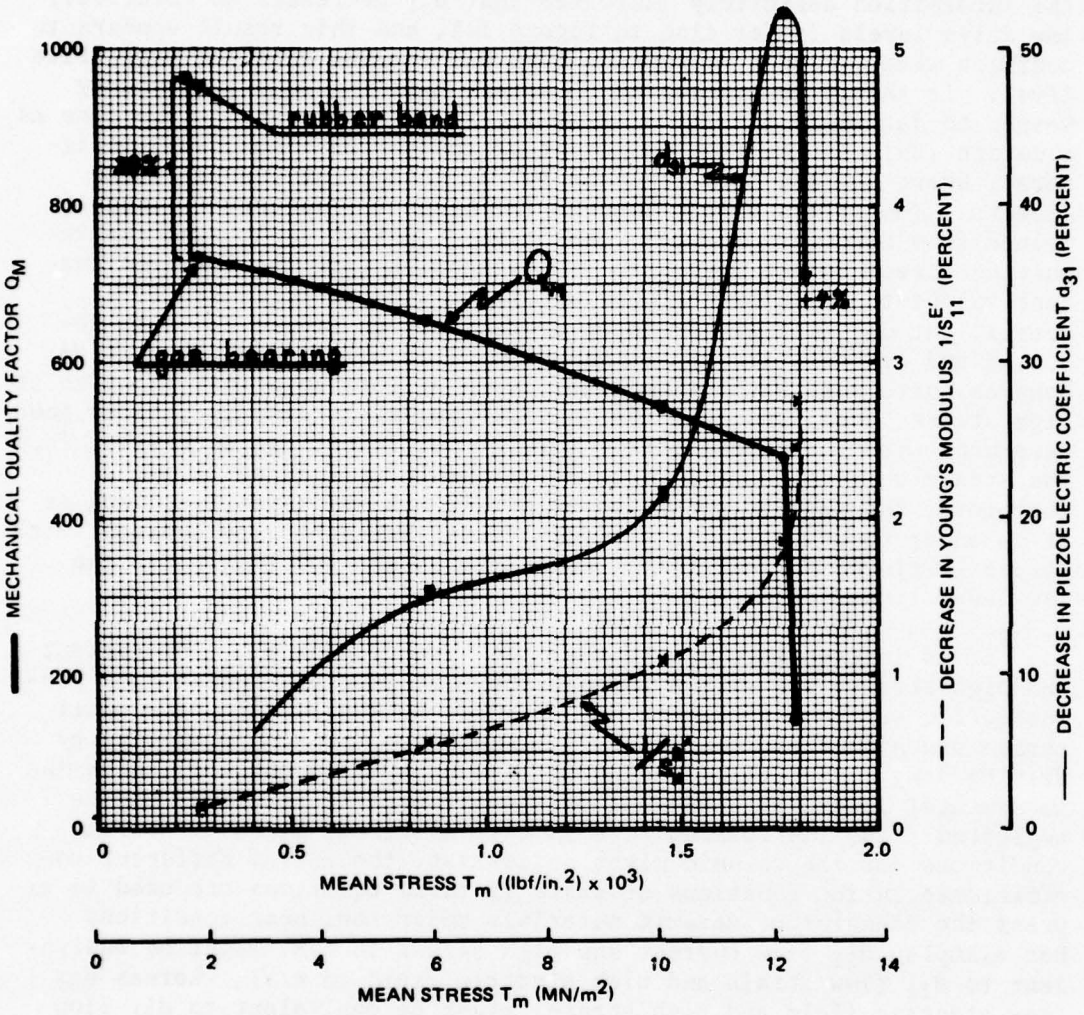

Figure 16. Mechanical Quality Factor, Decrease in Young's Modulus, and Decrease in Piezoelectric Coefficient versus Mean Stress for Ring B

The variation of d_{31} with stress is quite severe in figures 15 and 16, and there appears to be a region where the change becomes maximum -- although this observation cannot be considered factual inasmuch as the region is one of uncertainty (very near fracture). Nevertheless, the information definitely indicates that d_{31} decreases at relatively low drive levels (refer also to figure 14), and this result appears to conflict with Gerson's assumption that d_{31} remains constant with drive level. It should be remembered, however, that the equation used by Gerson to determine the stress from the measured current is the same as equation (2b), if the free component of the current ($\omega^E_T A \varepsilon^T_{33} E_3$) is ignored, where d_{31} has been replaced by d'_{31} to account for nonlinear effects. The stress values used in the present observations were obtained from directly measured quantities (equation (13)), and the resulting stress values were used in conjunction with the measured current values to compute the behavior of the piezoelectric stress coefficient d'_{31} with stress level as depicted in figure 17 (both abscissa and ordinate are in rms values). This plot indicates that d'_{31} behaves quite well with drive level, with slight variations in value at high stress level, and that the initial low level value is in very good agreement with the piezoelectric strain coefficient d_{31} determined from the strain versus electric field relationship in figures 11 and 12. Therefore, the results presented by Gerson are still valid as long as it is understood that it is d'_{31} (C/N) that is essentially constant with stress level and not d_{31} (m/V), whose values are equal only for the low-level linear case.

It is interesting to note that the variation in d'_{31} (low current and high stress) for ring A follows the same general trend as the piezoelectric strain coefficient d_{31} measured by Woollett[16] under small strain and high field conditions -- determined from equation (2a) by driving long, thin, thickness-poled bars at a frequency well below the fundamental length resonance of the bars where the stress T_1 may be neglected. The implication here is that different kinds of driving conditions for the ceramic might necessitate the use of different coefficients in the equations of state if these equations are used to express the behavior of ceramic materials under nonlinear conditions. For example, d'_{31} (low current and high stress in C/N) might be equivalent to d_{31} (low strain and high electric field in m/V), whereas d_{31} (low electric field and high strain) might be equivalent to d'_{31} (low stress and high current). If such a situation exists, then different symbols would probably be needed for the different sets of conditions.*

---

*No proof exists at present to substantiate such comments, which are made solely to activate the imagination of researchers in transducer ceramic studies.

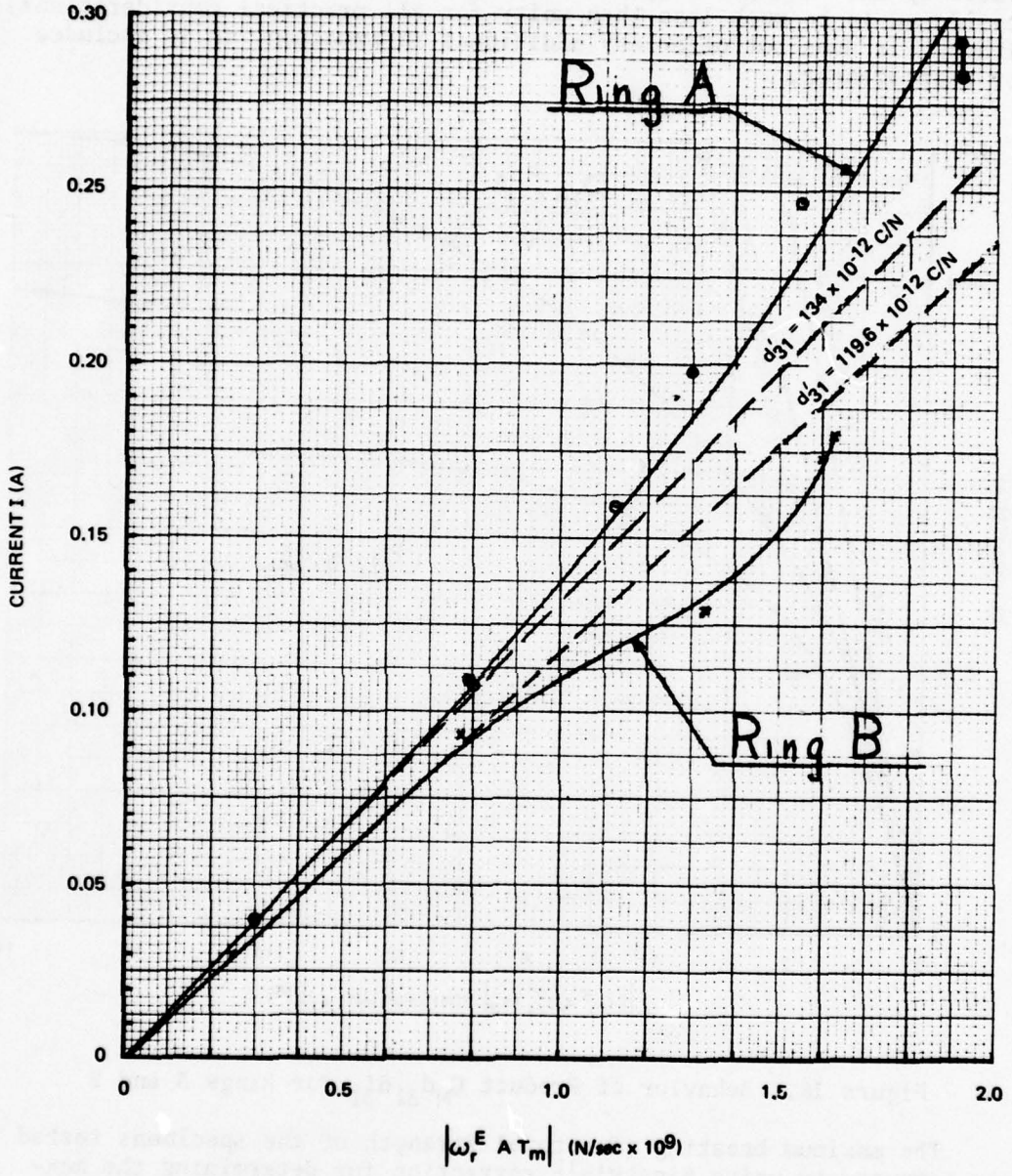

Figure 17. Behavior of Piezoelectric Stress Coefficient d'_{31} for Rings A and B

Figure 18 is a plot of the magnitude of equation (10) with s^E_{11} replaced by the real part s^E_{11} of its complex quantity (i.e., $1/Q_M$ was considered to be much less than unity for all practical considerations); although it does not offer any additional information, it is included for completeness.

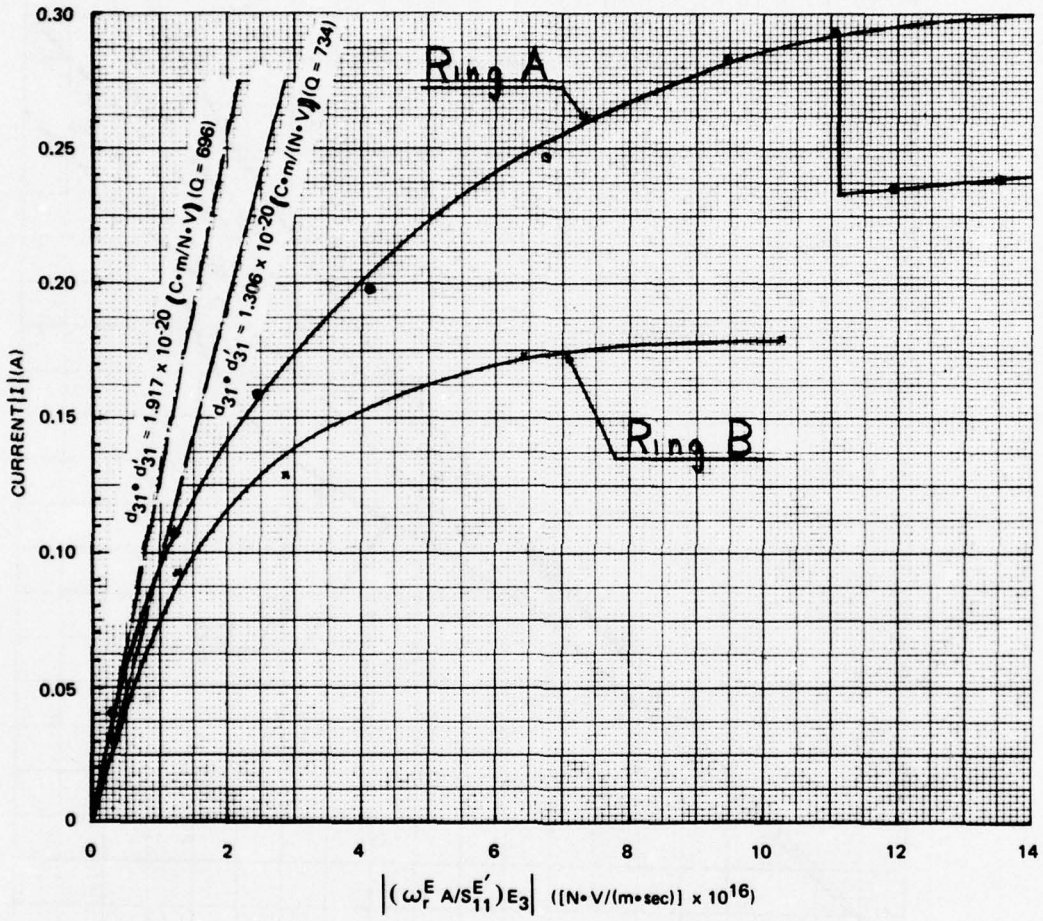

Figure 18. Behavior of Product $Q_M d_{31} d'_{31}$ for Rings A and B

The maximum breaking (fracture) strength of the specimens tested was computed by using Sinsky's[12] correction for determining the maximum strain at the inside radius of the rings from the strain at the outside radius of the rings (the correction for the dimensions of the rings used here and for $\sigma^E = 0.33$ was $S_a = (1.345)S_b$) and the value of

Young's modulus at fracture. Calculations for ring B were straightforward, but those for ring A had to be corrected for the influence of the cellophane insulator at the higher drive levels. Figure 19 is a plot of the resonance frequency of the rings versus the electric field level and was used to estimate the true resonance frequency at fracture for ring A (f_r^E = 18.255 kHz), from which Young's modulus was calculated by using equation (5). The fracture strain S_b (159 μm/m) for ring A was taken from the extended portion of the strain curve in figure 11, and that for ring B (S_b = 128 μm/m) was taken from the strain curve in figure 12. The maximum (peak) dynamic stress* was computed by using equation (13), with the mean values replaced by the values at r=a to yield 3550 lbf/in.^{2} (24.5 MN/m^2) and 2950 lbf/in.^{2} (20.3 MN/m^2) for rings A and B, respectively. If the low-level Young's modulus is used in the computations, the values are slightly higher -- 3690 lbf/in.^{2} (25.4 MN/m^2) and 3030 lbf/in.^{2} (20.9 MN/m^2). The computed stress limits are in agreement with Gerson's observations and with the dynamic values quoted by commercial manufacturers,[17] and are only 10 to 15 percent lower than the average dynamic fracture strengths quoted by Smith and Rice[18] for similar types of ceramic material (for Edo Western 4100 lbf/in.^{2} (28.3 MN/m^2) and for Channel 3300 lbf/in.^{2} (22.8 MN/m^2)). Other observers[13] have claimed values as high as 5000 to 6000 lbf/in.^{2} (34.5 to 41.4 MN/m^2) for the peak dynamic tensile strength of similar hard lead-zirconate-titanate ceramic supplied by a different manufacturer. All of the values quoted might conceivably be correct inasmuch as the ultimate stress level depends on such variables as manufacturing processes, age after polarization when the ceramic is tested, degree of pore concentrations in the ceramic, and heating effects at high drive level. Clarification of the influence of these variables on fracture strength can only be achieved through further measurements.

It should be noted that in all cases the dynamic fracture strength of Navy Type-I ceramic is about 50 or 60 percent of the static strength.[19]

---

*It should be noted that the rings actually broke at the next higher field level tried in the measurements but that the last observed field data point was the one used for stress fracture calculations. The quoted fracture levels are still valid, however, since fracture occurs in a region of strain (or stress) saturation.

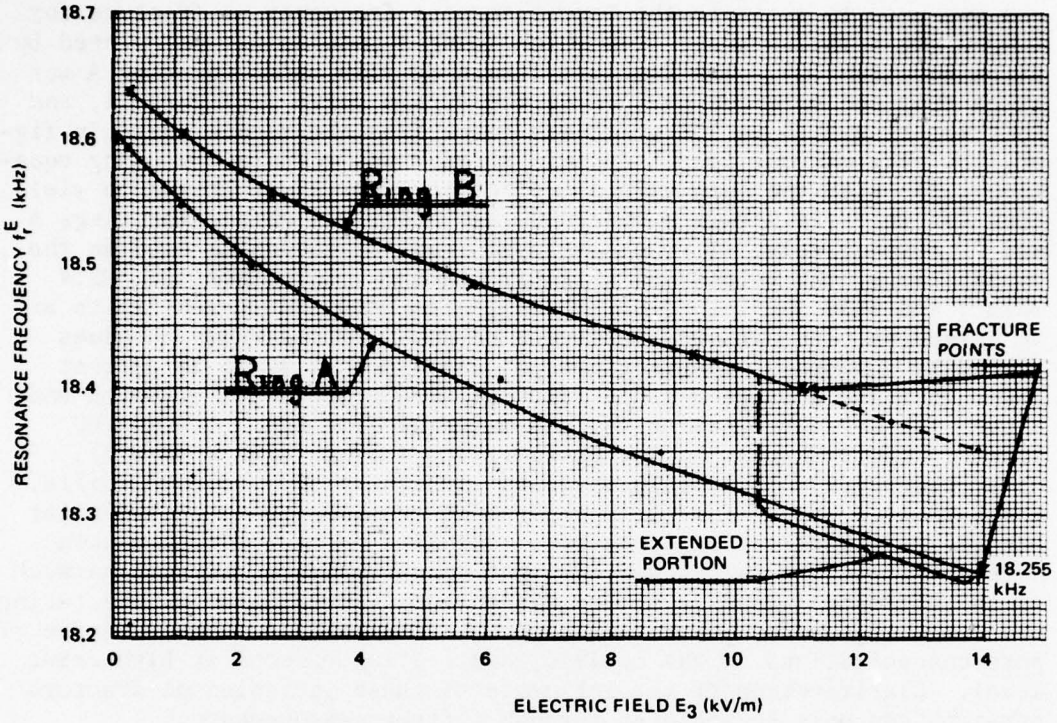

Figure 19. Resonance Frequency versus Electric Field for Rings A and B

NONLINEAR THEORETICAL ANALYSIS

The lack of an existing precise, practical, nonlinear mathmetical theory for predicting the behavior of piezoelectric ceramics in sonar transducers has been noted. The key word is sonar (sonic, as opposed to ultrasonic, frequencies), since ceramic properties useful to transducer design engineers are usually determined on specific geometric specimens (see figure 20) driven electrically at their fundamental resonance frequencies and sometimes at frequencies well below the fundamental resonance.

One phase of this investigation was to develop a simplified nonlinear theory that could be used to interpret the experimental data collected. A simplified mathematical approach is currently preferred

as a tool because of the complexity that would be involved if a rigorous continuum-physics approach[5] were used to analyze composite transducer structures and transducer arrays. Even a simplified approach to nonlinear theory involves considerable complication, but with appropriate assumptions and boundary conditions usable equations can be developed.

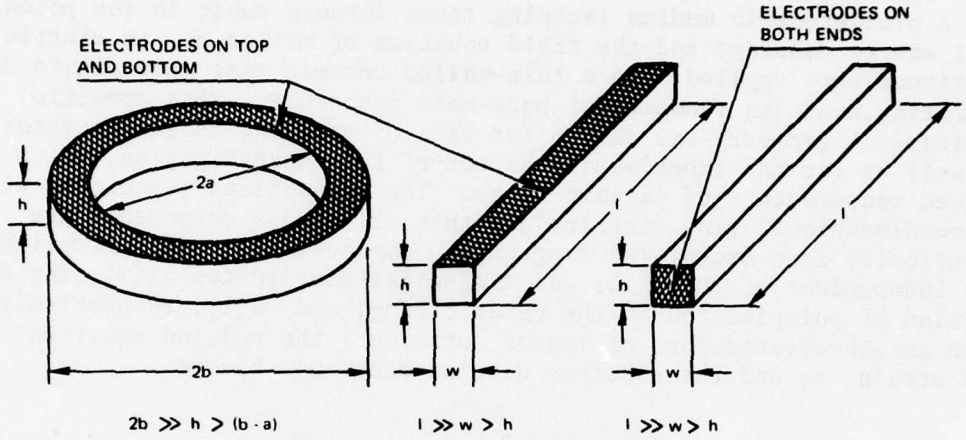

Figure 20. Typical Ceramic Test Specimens

APPROACH

An approach similar to that used for determining third-order piezoelectric coefficients[20] from ultrasonic measurement information will be followed. The same approach can not be used because at ultrasonic frequencies equations of state are usually written in terms of the elastic stiffness coefficients[21] c^E at constant electric field or c^D at constant electric displacement (which are the appropriate parameters measured with ultrasonic techniques), whereas the equations of state applicable to transducer theory (sonic frequencies) are usually written in terms of the elastic compliance coefficients s^E or s^D. Although there exists a relationship between s and c (with the appropriate superscripts),[22]

$$s_{ij} = \frac{(-1)^{i+j} \Delta c_{ij}}{\Delta c} \tag{14}$$

where Δ^c is the determinant of the c_{ij} terms and $\Delta^c{}_{ij}$ is the minor obtained by suppresssing the i-th row and j-th column, there appears to be some doubt as to its rigorousness if used to determine low frequency coefficients from the measured high frequency coefficients. In addition, equation (14) was derived from the linear constitutive equations of state and the problem being addressed here is a nonlinear one.

Therefore, the expanded nonlinear constitutive equations of state for a piezoelectric medium (keeping terms through cubic in the potential energy density) and the field equation of motion for an elastic continuum were applied[23] to a thin-walled ceramic ring (see figure 20) operating near its fundamental hoop-mode resonance. This specific cylindrical geometry was chosen for ease of applying nonlinear theory as well as for the experimental aspect of this investigation, which involved measurements of ceramic rings. The assumptions associated with a one-dimensional ring vibrator are that all stress components are identically zero except the tangential component T_1, and all variables are independent of the axial and tangential coordinates $z(3)$ (the direction of polarization in the ceramic ring) and $\theta(1)$, respectively; with an abbreviated form of tensor notation[21] the reduced equations for the strain η_1 and the electric displacement D_3 become

$$\eta_1 = s^E_{11}T_1 + d_{31}E_3 + \frac{1}{2}s^E_{111}(T_1)^2 + \frac{1}{2}d_{331}(E_3)^2 + d_{311}E_3T_1 \quad \text{and} \qquad (15)$$

$$D_3 = d_{31}T_1 + \epsilon^T_{33}E_3 + \frac{1}{2}d_{311}(T_1)^2 + \frac{1}{2}\epsilon^T_{333}(E_3)^2 + d_{331}E_3T_1, \qquad (16)$$

where

second-order coefficients s^E_{11}, d_{31}, and ϵ^T_{33} are the usual linear elastic, piezoelectric, and dielectric coefficients,

the remaining coefficients s^E_{111}, d_{331}, d_{311}, and ϵ^T_{333} are the nonlinear or third-order coefficients of the piezoelectric ceramic, and

$$\rho\,\frac{\partial^2 u_r}{\partial t^2} = -\frac{T_1}{\bar{r}} + \left(\frac{u_r}{\bar{r}}\right)\frac{T_1}{\bar{r}} + \left(\frac{\partial u_r}{\partial \bar{r}}\right)\frac{T_1}{\bar{r}} \quad \text{is the} \qquad (17)$$

approximate equation of motion for the ceramic ring.

The Lagrangian strain component η_1 in the tangential direction is given as

$$\eta_1 = \frac{u_r}{\bar{r}} + \frac{1}{2}\left(\frac{u_r}{\bar{r}}\right)^2 + \left(\frac{u_r}{\bar{r}}\right)\left(\frac{\partial u_r}{\partial \bar{r}}\right) . \tag{18}$$

When the nonlinear terms are ignored, equations (15) through (18) reduce to the common linear expressions. Reciprocity should not be assumed when nonlinear effects are present, but not doing so would only aggravate the already complex situation. The first step, therefore, is to see if a useful wave equation can be derived from the four nonlinear equations for a thin-walled ring.

When the ring is excited very near resonance, large stresses and strains are induced in the ring by low electric field levels because of the high Q_M of the material. The controlling parameters for this case are the elastic coefficients, and only the linear electric field term will be retained.* Under these conditions the stress becomes approximately[23]

$$T_1 \simeq -\frac{s_{11}^E}{s_{111}^E}\left\{1 \mp \sqrt{1 + 2\left(\frac{s_{111}^E}{\left(s_{11}^E\right)^2}\right)\left(\eta_1 - d_{31}E_3\right)}\right\} . \tag{19}$$

With the use of equation (18) the radical can be expanded (keeping terms to the order consistent with previous approximations) to yield

$$T_1 \simeq \frac{1}{s_{11}^E}\left(\frac{u_r}{\bar{r}}\right) + \frac{1}{2s_{11}^E}\left(1 - \frac{s_{111}^E}{\left(s_{11}^E\right)^2}\right)\left(\frac{u_r}{\bar{r}}\right)^2 + \frac{1}{s_{11}^E}\left(\frac{u_r}{\bar{r}}\right)\left(\frac{\partial u_r}{\partial \bar{r}}\right) - \frac{d_{31}}{s_{11}^E}E_3 \tag{20}$$

The last expression, in conjunction with equation (17), yields the nonlinear wave equation

$$\frac{d^2\eta}{dt^2} + \left(\omega_r^E\right)^2(1 - \gamma\eta)\eta = \left(\omega_r^E\right)^2 d_{31}E_3 , \tag{21}$$

---

*Note that equations (15) and (16) may also be used at very low frequencies ($T_1 \approx 0$) to obtain information about the third-order piezoelectric (d_{331}) and dielectric (ε_{333}^T) coefficients.

where

$$\omega_r^E = \frac{1}{r_m}\sqrt{\frac{1}{\rho s_{11}^E}},$$

$$\gamma = \frac{1}{2}\left(1 + \frac{s_{111}^E}{\left(s_{11}^E\right)^2}\right),$$

$$\eta = \frac{u_r}{r_m}, \text{ and}$$

$\bar{r} \equiv r_m$ (the mean radius of the ring).

The solution of equation (21) is by no means straightforward, if even possible. Two different approaches were tried in order to obtain information from the nonlinear wave equation. First, an approximate perturbation for the strain variable η was tried, and, second, an analog computer approach was used to obtain a solution.

PERTURBATION SOLUTION

It was initially assumed that the strain variable η could be written as the sum of two parts

$$\eta = \eta^{(0)} + \eta^{(1)}, \tag{22}$$

where

$\eta^{(0)}$ is the solution of the linear, unperturbed ($\gamma = 0$) equation and

$\eta^{(1)}$ is the remaining or perturbation part $\left(\left|\eta^{(1)}/\eta^{(0)}\right| << 1\right)$.

If it is assumed also that the electric field is sinusoidal ($E_3 = \mathcal{E}_3 e^{j\omega t}$), then $\eta^{(0)}$ and $\eta^{(1)}$ can be written as

$$\eta^{(0)} = \eta_m^{(0)} e^{j\omega t} \text{ and } \eta^{(1)} = \eta_m^{(1)} e^{j2\omega t} \tag{23}$$

where the maximum value of the fundamental component is

$$\eta_m^{(0)} = \frac{d_{31}\mathcal{E}_3}{\left[1 - \left(\frac{\omega}{\omega_r^E}\right)^2\right]} \tag{24}$$

and the maximum value of the second harmonic is

$$\eta_m^{(1)} = \frac{\gamma\left(\eta_m^{(0)}\right)^2}{\left[1 - 4\left(\frac{\omega}{\omega_r^E}\right)^2\right]} \quad . \tag{25}$$

In order to keep the strain components finite it is necessary to consider the linear compliance coefficient s_{11}^E as a complex quantity. Then equations (24) and (25) become, at $\omega = \omega_r^E$,

$$\eta_m^{(0)} = -jd_{31}Q_M\mathcal{E}_3 \text{ (see equation (7)) and}$$

$$\eta_m^{(1)} = -\frac{1}{3}\gamma\left(\eta_m^{(0)}\right)^2 , \tag{26}$$

assuming that Q_M is large ($4/Q_M \ll 3$). Therefore, it would appear that spectral analysis measurements of the relative level of second harmonic and absolute fundamental displacement components would yield information about the third-order elastic compliance coefficient s_{111}^E.

In addition, the current at resonance can be derived, retaining the second-order electric field term in equation (16), as

$$I = \left(\frac{d_{31}^2\omega_r^E A}{s_{11}^E}Q_M + j\omega_r^E A\varepsilon_{33}^s\right)E_3 + \left(-\frac{2\omega_r^E A d_{311}d_{31}^2}{\left(s_{11}^E\right)^2}Q_M + j\omega_r^E A\varepsilon_{333}^s\right)E_3^2 , \tag{27}$$

where ε_{333}^{s} has been defined as

$$\varepsilon_{333}^{s} = \varepsilon_{333}^{T} \left\{ 1 + \frac{d_{311} d_{31}^{2}}{\varepsilon_{333}^{T} \left(s_{11}^{E} \right)^{2}} - \frac{d_{31}^{2} Q_{M}^{2} d_{311}}{\varepsilon_{333}^{T} \left(s_{11}^{E} \right)^{2}} \left[1 + \frac{2 d_{31} s_{11}^{E}}{d_{311}} \left(1 - \frac{4}{3} \gamma \right) \right] \right\}. \tag{28}$$

Note that the leading (linear) term in equation (27) is the same as equation (9) when $d_{31}' = d_{31}$ and $\omega = \omega_r^E$, since

$$\varepsilon_{33}^{s} = \varepsilon_{33}^{T} \{ 1 - [d_{31}^{2} / (\varepsilon_{33}^{T} s_{11}^{E})] \}.$$

Since it is shown in appendix B that the fundamental blocked component ($I_b = j\omega_r^E A \varepsilon_{33}^{s} E_3$) of the input current is negligible, for all practical purposes, for ring measurements described in this report, it will be assumed that its counterpart in the second-harmonic component is also negligible. Under these conditions the current becomes

$$I = \frac{d_{31}^{2} \omega_r^E A Q_M}{s_{11}^{E}} E_3 - \frac{2 \omega_r^E A d_{311} d_{31}^{2} Q_M}{\left(s_{11}^{E} \right)^{2}} E_3^{2}, \tag{29}$$

which demonstrates that spectral analysis could be used to yield information about the third-order piezoelectric coefficient inasmuch as

$$\frac{I^{(1)}}{I^{(0)}} = \frac{2 d_{311} E_3}{s_{11}^{E}}, \tag{30}$$

where $I^{(1)}$ and $I^{(0)}$ are the magnitudes of the second-harmonic and fundamental current components, respectively.

Spectral analysis measurement of the radial displacements and input driving currents for the rings is difficult with conventional equipment because heating problems force the rings to be excited with low-duty-cycle pulses. Reliable measurement data would probably require sophisticated techniques, such as fast Fourier transform (FFT) processing. This aspect has not been thoroughly considered because it was felt that perturbation theory, although an improvement over linear theory and useful in explaining some aspects of nonlinear behavior,

would not be sufficient to explain the gross nonlinear effects experienced in the ring measurements. Therefore, the decision was made to try an alternative approach to the problem.

ANALOG COMPUTER SOLUTION

A preliminary analog computer solution was sought[24] in which the resulting response pulse shapes and jump phenomena would duplicate actual experimental observations. Duplication of complete ring behavior was not attempted because of insufficient time. Instead, the analog computer was programmed by using experimentally determined parameters from measurements of a single ring at a single driving field in order to demonstrate the capabilities of the analog computer.

The first predicament encountered was the necessity to incorporate some appropriate loss term in the wave equation to keep η finite. Since the loss parameter in a simple mechanical system is associated with the velocity component, it has been assumed that a term proportional to the time derivative of the second term on the left-hand side of equation (21) would account for nonlinear losses. Hence, equation (21) becomes

$$\frac{d^2\eta}{dt^2} + \beta(1 - 2\gamma\eta)\frac{d\eta}{dt} + (\omega_r^E)^2(1 - \gamma\eta)\eta = (\omega_r^E)^2 d_{31} E_3 , \qquad (31)$$

where

$$\beta \equiv \frac{\omega_r^E}{Q_M^E} \quad \text{and}$$

Q_M^E is the low-level mechanical quality factor measured under linear conditions.

When the nonlinear elastic parameter γ is zero, equation (31) reduces to the conventional form found in textbooks on mechanical vibrations.

Equation (31) was simulated on an Electronics Associates, Incorporated (EAI) 680 analog computer with the results shown in figure 21. Figure 21a shows measured pulse shapes for an actual ring; the upper trace is the applied voltage pulse, the middle trace is the resulting current pulse, and the bottom trace is the resulting radial displacement of the ring. The computer simulation at the same drive level is shown in figure 21b, where the upper trace is the driving pulse and the lower trace is the strain response to the driving pulse. Note that the displacement pulse in figure 21a has a strange shape. In all other measurements made on ceramic rings during this project it was found

that the displacement pulse shapes were almost identical to the current pulse shapes at the same drive levels. Hence, it seems reasonable to conclude that there was an instrumentation problem with the displacement probe in this particular case and, therefore, that comparison should be made between the analog strain pulse shape and the experimental current pulse shape. Further clarification of this point could not be made because the ring used for this study had fractured.

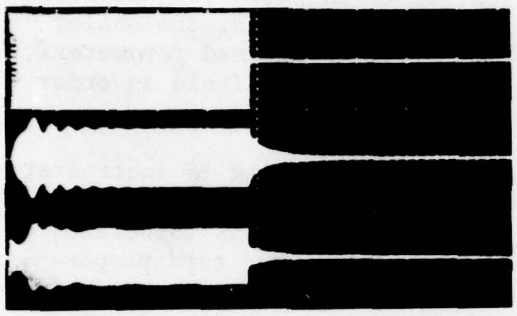

Figure 21a. Actual Voltage, Current, and Displacement

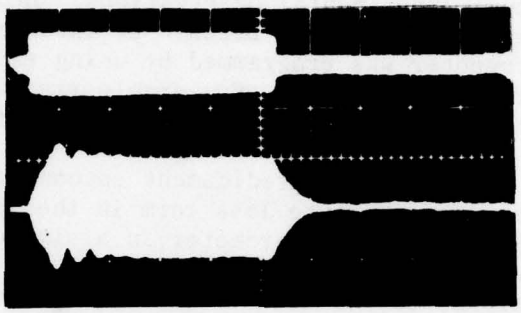

Figure 21b. Computer Generated Voltage and Strain-Response

Figure 21. Comparison of Computer - Generated Data with Experimental Data

It is interesting to note that all of the response pulses had ripples (similar to beat phenomena) that could not be eliminated by varying the frequency and that appeared to decrease exponentially with time. This phenomenon was not observed at the very low driving fields (linear behavior, see figure 7a) but became pronounced as the drive level increased (increased current and strain). This same phenomenon has been observed and discussed elsewhere[25] in the field of nonlinear ceramic studies.

Figure 22 depicts the real time spectrum of the steady-state portion of the analog strain pulse and shows the presence of second- and third-harmonic components at relative levels of -32 dB and -43 dB, respectively, below the fundamental component. Information of this nature could be useful in estimating the relative magnitude of the second harmonic to look for experimentally (if the results of the perturbation theory presented previously are applied at discrete drive levels for the rings).

Figure 23 illustrates the jump phenomenon that is so characteristic of nonlinear problems and that can be verified by referring to the

experimental results in figures 7e through 7g. Moving from left to right in figure 23, the simulated strain (≈displacement) responses for frequencies slightly below, at, and slightly above resonance are depicted. This sequence of events demonstrates a highly nonlinear situation since the magnitude of the strain is highly nonsymmetric about resonance. In addition, it should be noticed that the so-called beat phenomenon discussed previously is quite apparent here and that it also is highly nonsymmetric about resonance -- the effective number of beats being considerably less below resonance than at (and above) resonance.

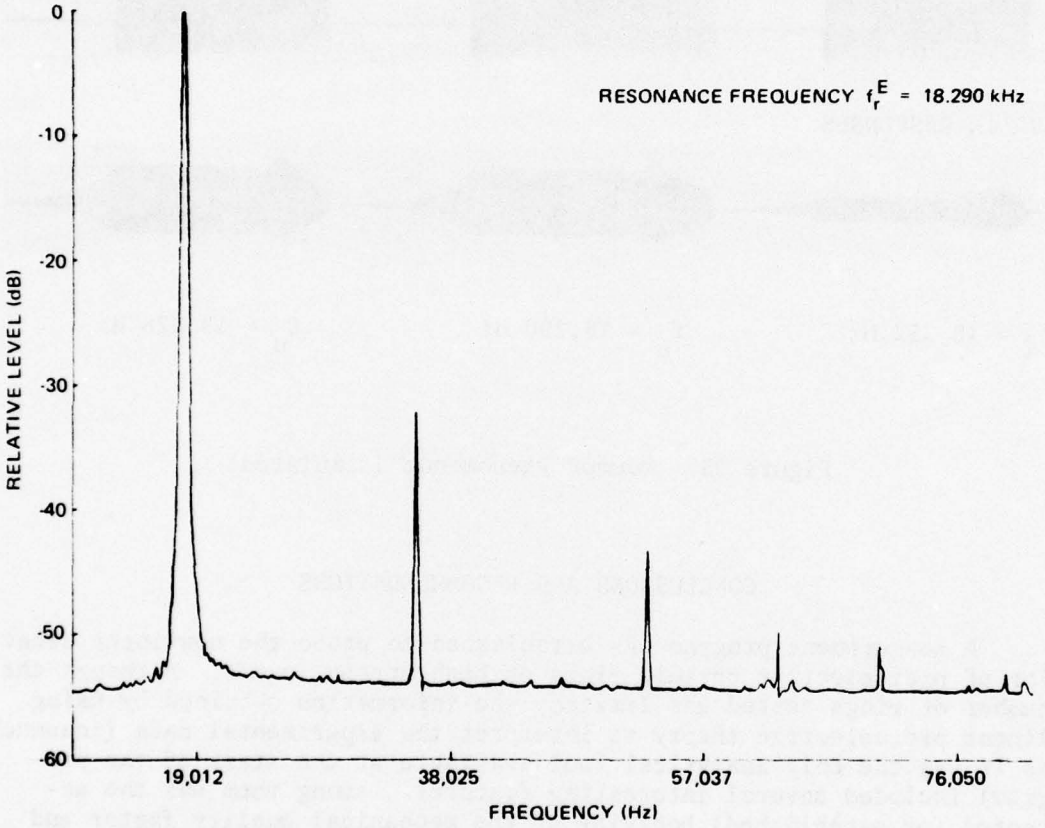

Figure 22. Spectrum of Simulated Steady-State Radial Displacement of Ring (resonance frequency f_r^E = 18.290 kHz)

It should be reemphasized at this point that the results presented in the latter part of this theoretical investigation are only preliminary in the sense that the analog computer solution was the last approach attempted and there was not sufficient time to completely evaluate

that approach to determine the nonlinear ceramic behavior. However, the demonstrated capability of an analog computer simulation to reproduce actual experimental data, including highly nonlinear behavior such as beat and jump phenomena, makes the use of the analog computer, in conjunction with derived theoretical results and experimental data, very encouraging for obtaining quantitative information about the nonlinear characteristics of piezoelectric ceramics.

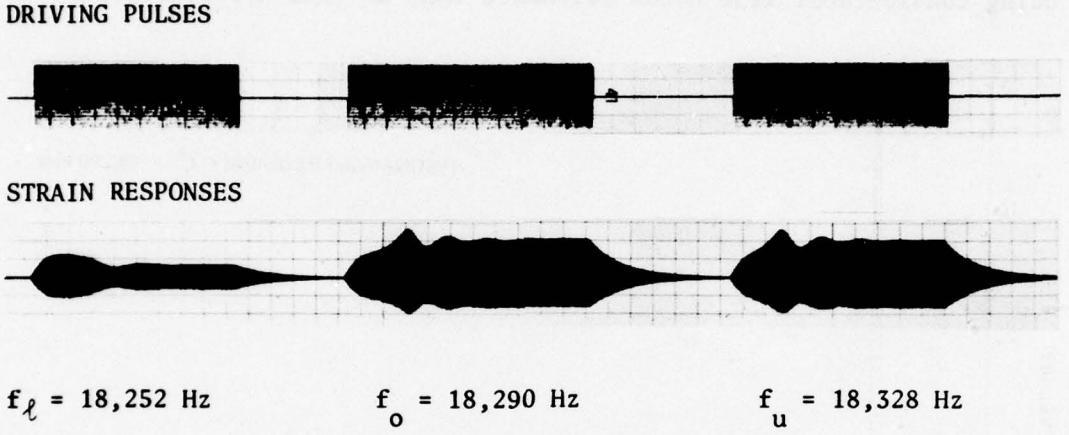

Figure 23. "Jump" Phenomenon (simulated)

CONCLUSIONS AND RECOMMENDATIONS

A measurement program was established to probe the nonlinear behavior of piezoelectric ceramic rings at high strain levels. Although the number of rings tested was limited, the information obtained by using linear piezoelectric theory to interpret the experimental data (inasmuch as it was the only analytical tool available at the start of the program) included several interesting features. Among them was the accepted (or established) behavior of the mechanical quality factor and of Young's modulus (of the ceramic) versus stress level. In addition, initial measurements indicated that the piezoelectric coefficient d_{31} commonly used in the equations of state for piezoelectric material does not obey reciprocity when nonlinear effects are present. It was tentatively found that the strain coefficient d_{31} ($\simeq S_1/E_3$) decreased with stress level, whereas d'_{31} ($\simeq D_3/T_1$) increased with stress level. These observations need to be verified by additional measurements on ceramic specimens supplied by other manufacturers; it was felt that the rings measured in this investigation exhibited exceptionally large nonlinear

effects that might not be typical of Navy Type-I ceramics. Also, the measurement scheme should be improved to account for phase information and possible spectral-analysis measurements. The potential problems associated with the present measurement system need to be better understood and corrected where possible (for example, by improving the gas-bearing assembly to eliminate unwanted losses).

Theoretical analysis of the nonlinear behavior of a piezoelectric ceramic ring demonstrated the complications involved in finding a general solution for predicting high-level nonlinear behavior in ceramics. However, a reduced nonlinear differential equation developed for the ceramic ring was programmed on an analog computer, and the resulting outputs were strikingly similar to actual experimental data. These kinds of results, compared with the complex aspects of a generalized nonlinear theory, indicate that analog computer techniques may be the only convenient means of interpreting and understanding ceramic nonlinear behavior. The analog computer solution must be matched with actual driving conditions and measurement data on ceramic rings before quantitative information can be obtained about the nonlinear elastic and piezoelectric parameters.

REFERENCES

1. Physical Acoustics, vol. 1, part A, W. P. Mason, ed., Academic Press, New York, 1964, p. 169.

2. R. S. Woollett and C. L. LeBlanc, "Ferroelectric Nonlinearities in Transducer Ceramics," IEEE Transactions on Sonics and Ultrasonics, vol. SU-20, no. 1, January 1973, p. 24.

3. Katsuo Negishi, "Jump Phenomenon in Resonance Curve of Ferroelectric Ceramic," Journal of the Physical Society of Japan, vol. 15, no. 3, March 1960, p. 534.

4. N. W. McLachlan, Ordinary Nonlinear Differential Equations, Clarendon Press, Oxford, England, 1950, p. 60.

5. H. F. Tiersten, "On the Nonlinear Equations of Thermo-Electroelasticity, "International Journal of Engineering Science, vol. 9, 1971, pp. 587-604.

6. "Piezoelectric Ceramic For Sonar Transducers," MIL-STD-1376 (SHIPS), 21 December 1970.

7. J. F. Haskins and J. L. Walsh, "Vibrations of Ferroelectric Cylindrical Shells with Transverse Isotropy. I. Radially Polarized Case," Journal of the Acoustical Society of America, vol. 29, no. 6, June 1957, pp. 729-734.

8. "An Evaluation of Commercial Navy Type I Sonar Ceramics," Materials Panel of the MOST Technical Committee on Transducers and Hydromechanics report for Naval Sea Systems Command, August 1974.

9. "Low Pressure Air Bearing," Interand Corporation publication, Rockville, Maryland.

10. R. Gerson, "Dependence of Mechanical Q and Young's Modulus of Ferroelectric Ceramics on Stress Amplitude," Journal of the Acoustical Society of America, vol. 32, no. 10, October 1960, pp. 1297-1301.

11. Proceedings of the Symposium on Nonlinear Circuit Analysis, J. Fox, ed., Polytechnic Institute of Brooklyn, December 1953.

REFERENCES (Cont'd)

12. J. A. Sinsky, "Accuracy of Simple Approximations Used to Calculate Axially Symmetric Extensional Vibrations of Elastic Ring Transducer," IEEE Transactions on Sonics and Ultrasonics, vol. SU-21, no. 1, January 1974, pp. 45-49.

13. K. E. Feith, G. S. Kerr, and R. J. Taylor, "Large-Amplitude Piezoelectric Properties of Standard and Whisker-Reinforced Lead Zirconate-Titanate Ceramics," Journal of the Acoustical Society of America, vol. 51, no. 1 (part 1), January 1972, pp. 129-130 (A).

14. H. H. A. Krueger, "Stress Sensitivity of Piezoelectric Ceramics; Part 3. Sensitivity to Compressive Stress Perpendicular to the Polar Axis," Journal of the Acoustical Society of America, vol. 43, no. 3, March 1968, pp. 583-591.

15. G. E. Martin, "Dielectric, Elastic, and Piezoelectric Losses in Piezoelectric Materials," IEEE Transactions on Sonics and Ultrasonics, vol. SU-22, no. 3, May 1975, p. 241 (A).

16. R. S. Woollett, "Measurement of the Dissipation Associated with the Electromechanical Coupling in Piezoelectric Ceramics," National Technical Information Service, AD 657169, 12 July 1967.

17. "Piezoelectric Technology Data for Designers," Clevite Corporation Piezoelectric Division publication.

18. P. L. Smith, and R. W. Rice, "The Dynamic Strength of Standard Rings of Navy Type I Ceramic," NRL Report to NAVSHIPS (PMS 302-4), 8 Dec 1972.

19. C. L. LeBlanc, "NUSC Measurements on Standard Navy Type I Ceramic," NUSC Technical Memorandum TD12-469-73, 12 November 1973.

20. V. E. Ljamov, "Nonlinear Acoustical Parameters of Piezoelectric Crystals," Journal of the Acoustical Society of America, vol. 52, no. 1 (part 2), July 1972, pp. 199-202.

21. "Standards on Piezoelectric Crystals, 1949," Proceedings of the IRE, vol. 37, no. 12, December 1949, p. 1378.

22. W. P. Mason, Physical Acoustics and the Properties of Solids, D. Van Nostrand Co., Inc., Princeton, New Jersey, 1958, p. 361.

REFERENCES (Cont'd)

23. R. W. Dunham, Nonlinear Theory for a Thin-Walled Piezoelectric Ceramic Ring Excited in the Radial Breathing Mode, NUSC Technical Report 4971, 3 September 1975.

24. R. W. Dunham, "A Preliminary EAI 680 Analog Solution for the Nonlinear Behavior of a Piezoelectric Ceramic Ring Excited in the Radial Breathing Mode," NUSC Technical Memorandum TD12-181-75, 2 June 1975.

25. J. Pasternak and P. L. Smith, "A Linear Piezoelectric Vibrator Under Tone Burst Excitation," NRL progress report, February 1975.

APPENDIX A

INFLUENCE OF AMPLIFIER IMPEDANCE ON Q_M

The piezoelectric ceramic ring vibrator, being essentially a one-dimensional vibrator near the hoop-mode resonance frequency, can be represented by an equivalent circuit consisting of a blocked capacitance C_b in parallel with a series RCL branch (see figure A-1). The mechanical quality factor for such a circuit is usually expressed in terms of the electrical boundary conditions. More explicitly, for short-circuit electrical conditions (e(t) = 0)

$$\omega_r = \omega_r^E = \frac{1}{\sqrt{L_y C_y}} \quad \text{and} \quad Q_M = Q_M^E = \frac{1}{\omega_r^E C_y R_y} \quad \text{and} \tag{A-1}$$

for open-circuit electrical conditions (I=0)

$$\omega_r = \omega_r^I = \frac{1}{\sqrt{L_y \frac{C_b C_y}{(C_b + C_y)}}} = \frac{\omega_r^E}{\sqrt{1 - k^2}} \quad \text{and}$$

$$Q_M = Q_M^I = \frac{Q_M^E}{\sqrt{1 - k^2}} , \tag{A-2}$$

where k is the electromechanical coupling coefficient of the circuit and is defined as

$$k = \sqrt{\frac{C_y}{C_b + C_y}} . \tag{A-3}$$

The problem encountered in this investigation was to determine what happens to the quality factor of the circuit when the driving voltage e(t) is replaced by its equivalent voltage source and internal impedance. This type of problem is encountered when the source voltage is suddenly terminated and the current is allowed to decay through all impedance elements in the circuit, including the source impedance -- as

when measuring ceramic properties from current decay phenomenon, which is the case at hand.

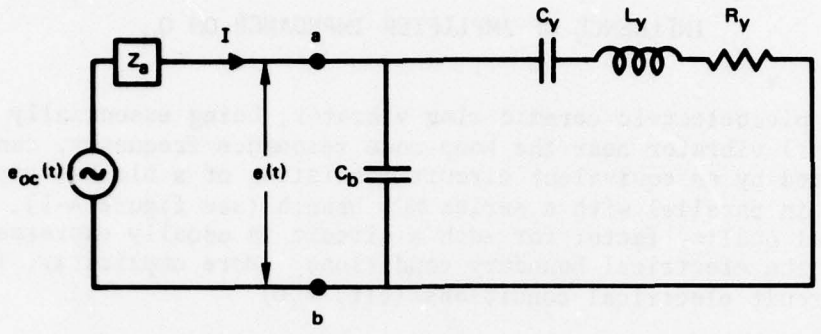

Figure A-1. Electromechanical Equivalent Circuit for Ceramic Ring Vibrator with Amplifier

The driving voltage e(t) may be represented by using Thevenin's theorem for any two-terminal linear network, as a generator equal to the open-circuit voltage appearing between the terminals a and b in series with an equivalent output impedance Z_a. This representation will be used to investigate the influence of the impedance of the power amplifier (which is, in reality, a nonlinear device) on the quality factor of an RCL circuit; the scheme is commensurate with analyzing nonlinear behavior of piezoelectric ceramic through linear equations.

Amplifier impedance is generally considered to be a complex quantity, whose magnitude varies with the operating frequency as well as with the load impedance. Inasmuch as the exact components of the amplifier impedance were not known, it was assumed that the impedance was a real number (resistive component R_a) in order to discover what influence even this simple condition would have on the quality factor of the circuit; two approaches were used. First, the quality factor was determined by simply considering the effects of an additional resistance in a simplified circuit under steady-state conditions. Second, the quality factor of a similar circuit under "pulse-driving" conditions was determined from the current decay in the circuit during the "off-time" of the electrical driving signal.

THE STEADY-STATE CASE

The circuit in figure A-1, with Z_a replaced by R_a and $e_{oc}(t)$ set equal to zero, may be revised to yield the more simplified circuit in figure A-2,

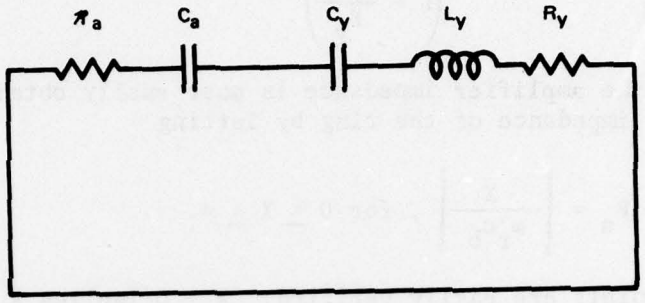

Figure A-2. Simplified Equivalent Circuit for Ceramic Ring Vibrator and Amplifier

where

$$R_a = \frac{\frac{1}{R_a}}{\left[\left(\frac{1}{R_a}\right)^2 + \left(\omega_r C_b\right)^2\right]} \quad \text{and}$$

$$C_a = \frac{\left[\left(\frac{1}{R_a}\right)^2 + \left(\omega_r C_b\right)^2\right]}{\omega_r^2 C_b} \quad . \qquad \text{(A-4)}$$

The resonance frequency and quality factor for the revised circuit are now defined as

$$\omega_r^2 = \frac{1}{L_y C} = \left(\omega_r^E\right)^2 \left(1 + \frac{C_y}{C_a}\right),$$

where

$$C = \frac{C_a C_y}{C_a + C_y} \quad , \text{ and} \qquad \text{(A-5)}$$

$$Q_M = \frac{\omega_r L_Y}{\left(R_Y + R_a\right)} = \frac{\left(\frac{\omega_r}{\omega_r^E}\right) Q_M^E}{\left(1 + \frac{R_a}{R_y}\right)} \quad . \tag{A-6}$$

Adjustment of the amplifier impedance is most easily obtained in terms of the blocked impedance of the ring by letting

$$R_a = \left| \frac{X}{\omega_r C_b} \right| \text{ , for } 0 \leq X \leq \infty. \tag{A-7}$$

The end points are easily verified: $X \to 0$ implies $R_a \to 0$ and $C_a \to \infty$ $[1/(\omega_r C_a) \to 0]$ such that the only remaining circuit elements are C_Y, L_Y, and R_Y, which yield the short-circuit electrical results stated in equation (A-1); and $X \to \infty$ implies $R_a \to 0$ and $C_a \to C_b$ such that the remaining circuit elements are C_b, C_Y, L_Y, and R_Y, which yield the open-circuit electrical results stated in equation (A-2).

The objective is to determine what happens to the resonance frequency and quality factor of the circuit for intermediate values of X (or R_a). The answer is obtained by rearranging and evaluating equations (A-5) and (A-6) in terms of the variable X as follows --

$$\left(\frac{\omega_r}{\omega_r^E}\right)^2 = 1 + \left(\frac{k^2}{1 - k^2}\right)\left(\frac{X^2}{1 + X^2}\right) \tag{A-8}$$

and

$$Q_M = \frac{\left(\frac{\omega_r}{\omega_r^E}\right) Q_M^E}{\left[1 + Q_M^E \left(\frac{\omega_r^E}{\omega_r}\right)\left(\frac{k^2}{1 - k^2}\right)\left(\frac{X}{1 + X^2}\right)\right]} \quad . \tag{A-9}$$

Evaluation of equation (A-8) indicates that the resonance frequency ω_r begins at ω_r^E and asymptotically approaches $\omega_r^E/\sqrt{1-k^2} = \omega_r^I$ as X increases positively from zero to infinity. For the ceramic ring case, where $k \approx 0.3$, the variation between extreme resonance points is only 5 percent and, therefore, may be considered constant for all practical purposes and equated to unity in evaluating equation (A-9). With this assumption, and using values that are representative of the ceramic rings measured in this investigation (f_r^E = 20 kHz, Q_M^E = 500, k = 0.3, and $C_b \approx 10^{-9}$ F), equation (A-9) is plotted in figure A-3 as a function of the dimensionless variable X. The plot is shown to be symmetrical about X = 1, but this is due to having neglected the slight increase in the ratio ω_r/ω_r^E as X increases. The dotted portion of the curve is intended to account for the slight 5 percent increase in Q_M above Q_M^E as X becomes infinite (to agree with equation (A-2)). The quality factor drops to a minimum ($Q_M \approx 20$) when X = 1, or when the amplifier impedance equals the impedance of the blocked branch of the ceramic ring, about 8 kΩ at ω_r^E. The same conclusion can be deduced directly from equation (A-9) by simply maximizing the term in the denominator containing X (specifically, differentiate $X/(1+X^2)$ with respect to X, set the result equal to zero, and solve for X).

The nonlinear variation of Q_M versus amplifier impedance, even if applied to the cases under consideration in this report, would not be as critical as the plot indicates inasmuch as the amplifier impedance was much less than the blocked impedance of the rings. This fact was verified by making some quick measurements with the 200-W MacIntosh amplifier. The 66-Ω tap on the output of the amplifier was used and corresponded to the expected impedance of the rings at resonance. The open-circuit voltage $e_{oc}(t)$ and the voltage $e(t)$ across several load resistors R_L were measured at three discrete frequencies, and the magnitude of the amplifier impedance $|Z_a|$ was determined from the equation

$$|e(t)| = |e_{oc}(t)| \frac{R_L}{(R_L + R_a)}, \text{ where } R_a \equiv |Z_a|. \qquad \text{(A-10)}$$

The measurements were made by using continuous wave excitation, and the magnitudes of the voltages were determined just before clipping appeared in the output signal. The data are listed in table A-1 and indicate that at the ring operating frequency of 18.5 kHz, which is near the upper limit of the amplifier, the amplifier impedance is approximately 20 Ω for a load resistance of 100 Ω. If this value were assumed to be a real number, independent of frequency, as was assumed for figure A-3, then the corresponding Q_M would be 445, or 90 percent of the short-circuit value. The measurements also indicate that the correction would be even less for the rings at high drive levels because $|Z_a|$ decreases with increased load resistance (Q_M for the ceramic decreases with increased drive level).

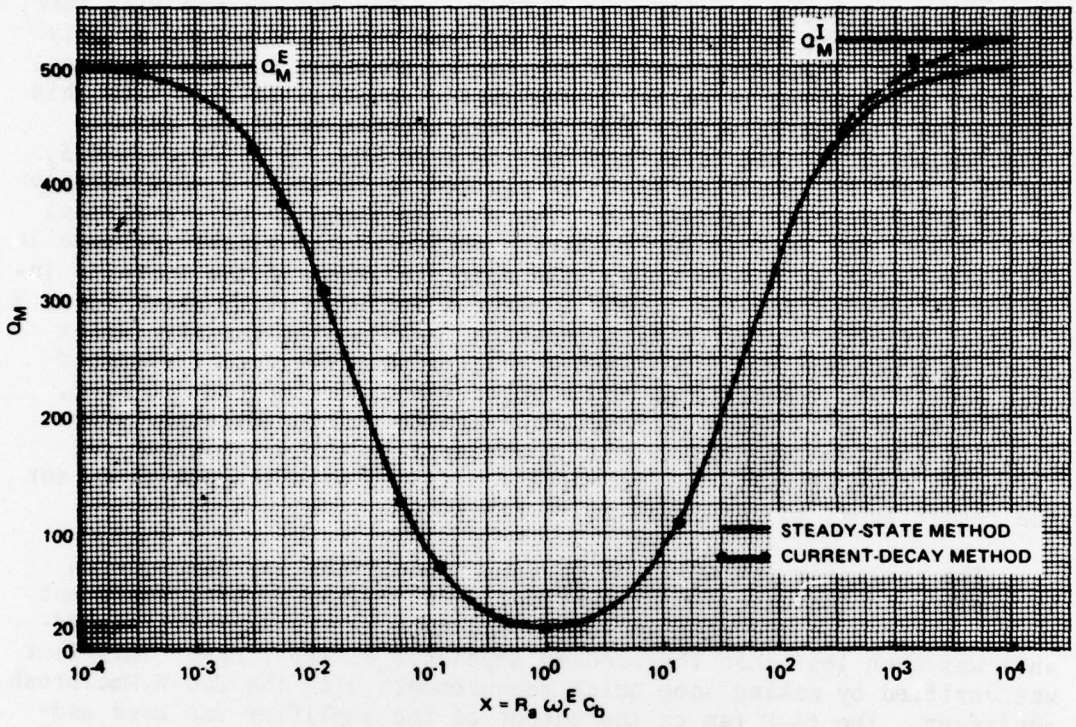

Figure A-3. Quality Factor Q_M versus Amplifier Impedance $\left(f_r^E = 20 \text{ kHz}, Q_M^E = 500, k = 0.3, \text{ and } C_b \approx 10^{-9} \text{ F}\right)$

The results of the analysis can only be used in a qualitative sense because the constraints imposed on the amplifier impedance did not include any frequency dependence nor the fact that the amplifier was actually used in a pulse mode. A more rigorous analysis could have accounted for the reactive components of the amplifier impedance, but quantitative results could not have been established without an extensive measurement program to determine the true amplifier impedance components at different frequencies and load levels. Since this was not done in the present circumstance, it will be assumed that the influence of the amplifier impedance on determining the quality factor of the ceramic rings at resonance is negligible.

Table A-1. Measured Values of Amplifier Impedance (200-W MacIntosh)

Frequency f_r (kHz)	Open-Circuit Voltage $e_{oc}(t)$ (Vrms)	Load Resistance R_L (Ω)	Voltage Across Load $\|e(t)\|$ (Vrms)	Plate Current i_p (mA)	Amplifier Impedance (Ω) ($R_a \equiv \|Z_a\|$)
1.0	185	1	2	450	91.5
		51	90	450	51.5
		100	140	400	32
		500	180	110	14
10.	190	1	2.05	450	91.7
		51	88.5	450	58.5
		100	137.	375	40
		500	185.	160	13.5
18.5	165	1	2.15	450	75.7
		51	88	450	44.6
		100	137	400	20
		500	165	210	--

THE CURRENT-DECAY CASE

The influence of the amplifier impedance, under the same restrictions introduced in the previous case (namely, that the impedance could be represented by a real number R_a), was also analyzed by using Laplace transformation techniques. The circuit in figure A-1 still applies with, as before, Z_a replaced by R_a and $e_{oc}(t)$ set equal to zero. The two loop equations for the circuit then become simply

$$0 = i_1 R_a + \frac{1}{C_b}\left[\int i_1 dt - \int i_2 dt\right] \qquad \text{(A-11)}$$

and

$$0 = i_2 R_Y + L_Y \frac{di_2}{dt} + \frac{1}{C_Y}\int i_2 dt + \frac{1}{C_b}\left[\int i_2 dt - \int i_1 dt\right], \qquad \text{(A-12)}$$

where i_1 and i_2 are the instantaneous currents in the two loops. The intent is to determine the decay behavior of i_1, which was monitored as the voltage drop across a 1-Ω resistor placed in series with the ring impedance and the low (ground) terminal of the amplifier. This additional resistor appears in loop one and may be effectively accounted for by letting $R_a = (R_a + 1)$ in any calculations.

The result of applying the Laplace transform to equations (A-11) and (A-12) and rearranging terms is

$$I_1(s)\left[R_a + \frac{1}{sC_b}\right] - I_2(s)\left(\frac{1}{sC_b}\right) = \frac{1}{sC_b}\left[i_2^{(-1)}(0^+) - i_1^{(-1)}(0^+)\right] \tag{A-13}$$

and

$$-I_1(s)\left(\frac{1}{sC_b}\right) + I_2(s)\left[R_Y + sL_Y + \frac{1}{sC_Y} + \frac{1}{sC_b}\right] = L_Y i_2(0^+) - \frac{1}{sC_Y}\left(i_2^{(-1)}(0^+)\right) - \frac{1}{sC_b}\left[i_2^{(-1)}(0^+) - i_1^{(-1)}(0^+)\right]. \tag{A-14}$$

Initial conditions must be specified for the circuit and will be established by using the information contained in figure A-4. Since $e(t) = E_o\cos(\omega_r^E t)$ appears across both branches of the circuit during steady-state operation, then

$$i_2(t) = \frac{E_o}{R_Y}\cos(\omega_r^E t) \text{ at } \omega_r^E = \frac{1}{\sqrt{L_Y C_Y}} . \tag{A-15}$$

The voltage across the inductance L_Y is

$$L_Y \frac{di_2}{dt} = -\omega_r^E L_Y \frac{E_o}{R_Y}\sin(\omega_r^E t), \tag{A-16}$$

which is equal and opposite in sign to the voltage across the capacitance element C_Y. Therefore, at $t = 0$, the intial conditions can be expressed as

$$i_2^{(-1)}(0^+) = q_Y(0^+) = 0, \qquad i_2(0^+) = \frac{E_o}{R_Y} , \tag{A-17}$$

and

$$i_1^{(-1)}(0^+) - i_2^{(-1)}(0^+) = q_1(0^+) - q_2(0^+) = q_b = E_o C_b \ ,$$

where q designates electrical charge.

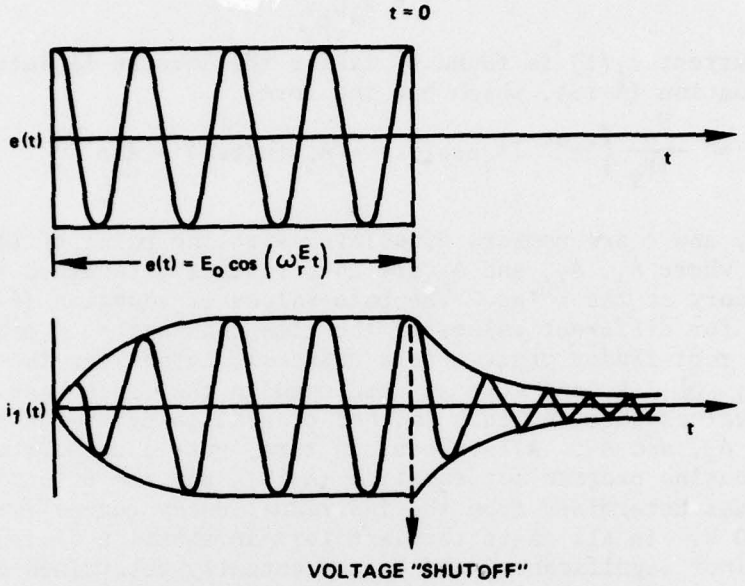

Figure A-4. Voltage and Current Waveforms

Equations (A-13) and (A-14) can now be solved for $I_1(s)$, by using the initial conditions in equation (A-17), to obtain

$$I_1(s) = \frac{\frac{E_o}{\tau R_Y}\left\{\left(s + \frac{\omega_r^E}{Q_M^E}\right) - \frac{(1 - k^2)}{\omega_r^E Q_M^E k^2}\left(s^2 + \frac{\omega_r^E}{Q_M^E}\, s + \omega_r^{I\,2}\right)\right\}}{\left\{\left(s + \frac{1}{\tau}\right)\left(s^2 + \frac{\omega_r^E}{Q_M^E}\, s + \omega_r^{I\,2}\right) - \frac{(\omega_r^E k)^2}{\tau(1 - k^2)}\right\}}, \qquad \text{(A-18)}$$

where

$$\omega_r^I = \frac{\omega_r^E}{\sqrt{1 - k^2}} \ ,$$

$$Q_M^E = \frac{\omega_r^E L_Y}{R_Y} = \frac{1}{\omega_r^E C_Y R_Y},$$

and

$$\tau = R_a C_b.$$

The current $i_1(t)$ is found by taking the inverse Laplace transform of equation (A-18), which has the form

$$i_1(t) = \frac{E_o}{\tau R_Y}\left\{2e^{at}\,[A_1\cos(bt) - A_2\sin(bt)] - A_3 e^{ct}\right\}, \qquad \text{(A-19)}$$

where a, b, and c are numbers associated with the poles of equation (A-18) and where A_1, A_2, and A_3 are coefficients determined by using residue theory at the poles. The pole values of equation (A-18) were determined for different values of the time constant τ by using the polynomial root finder program on a desk calculator* for the same values of f_r^E, Q_M^E, k, and C_b as were used in the first case. The resulting values were fed into another program to determine the coefficients A_1, A_2, and A_3. All values, in turn, were incorporated into a plotting routine program for equation (A-19), and the effective quality factor Q_M was determined from the individual decay curves for R_Y = 100 Ω and E_o = 10 V. In all cases the last term in equation (A-19) was found to be of minor significance, and Q_M was actually determined from the leading term in the equation. Table A-2 lists some of the values obtained by using this approach, and it should be noted that the frequency coefficient lies between ω_r^E (1.2566 x 10^5 Hz) and ω_r^I (1.3173 x 10^5 Hz) as R_a increases. The Q_M values obtained were superimposed on figure A-3 to demonstrate the agreement between the two methods.

The agreement between methods should be as good in general as that shown here since the same circuit and circuit elements were analyzed in both cases. Even though the behavior of Q_M versus amplifier impedance is highly nonlinear over the broad range of values considered, at any discrete value the circuit elements are fixed and linear analysis is valid. The agreement demonstrated that current decay measurements could indeed be used to predict the quality factor variation for ceramic rings as long as other practical considerations mentioned in the text (such as dependence of Q_M on decaying stress level) are not disregarded.

---

*Hewlett-Packard model 9820-A

Table A-2. Values for Q_M versus R_a

Amplifier Impedance R_a	Decay Coefficient $a(x10^2)$	Frequency Coefficient $b(x10^5)$	c	Effective Quality Factor Q_M
10^{-4}	-1.25	1.2566	-10^{13}	500
10^{-1}	-1.26	1.2568	-10^{10}	499.8
25	-1.45	1.2569	$-4x10^7$	433
50	-1.65	1.2569	$-2x10^7$	380
10^2	-2.00	1.2569	$-1x10^7$	308
$5.0x10^2$	-5.00	1.2570	$-2x10^6$	126
10^3	-9.00	1.2582	$-1x10^6$	70
$8.0x10^3$	-32.31	1.2890	$-12x10^4$	19.4
10^5	-5.70	1.3170	$-9x10^3$	110
10^7	-1.30	1.3171	$-9x10^1$	507
10^{10}	-1.25	1.3173	$-9x10^{-2}$	524

$\omega_r^E = 2\pi(20x10^3)$ Hz	$R_Y = 100\ \Omega$
$Q_r^E = 500$	$E_o = 10$ V
$k = 0.3$	$C_b = 10^{-9}$ F

APPENDIX B

DETERMINATION OF TOTAL CURRENT

The expression for the total current I into the ceramic ring is given by equation (9) in the text, which is (repeated for convenience)

$$I = j\omega A \frac{\dfrac{d_{31}d'_{31}}{s^E_{11}}}{\left[1 - \left(\dfrac{\omega}{\omega^E_r}\right)^2 \left(1 - \dfrac{j}{Q_M}\right)\right]} E_3 + j\omega A \varepsilon^T_{33} \left(1 - \frac{d_{31}d'_{31}}{\varepsilon^T_{33} s^E_{11}}\right) E_3. \qquad \text{(B-1)}$$

If it is assumed that $1/Q_M < 1$ or that s^E_{11} can be represented as a real number, then at resonance equation (B-1) reduces to

$$I = \frac{\omega^E_r A d_{31} d'_{31} Q_M}{s^E_{11}} E_3 + j\omega^E_r A \varepsilon^s_{33} E_3, \qquad \text{(B-2)}$$

where the blocked permittivity is defined for linear conditions as

$$\varepsilon^s_{33} = \varepsilon^T_{33} (1 - k^2) . \qquad \text{(B-3)}$$

The quantities in equation (B-2) can be further redefined to yield

$$I = \frac{E_o}{R_Y} + j\omega^E_r C_b E_o, \qquad \text{(B-4)}$$

which shows that the input current is composed of a blocked component ($I_b = j\omega^E_r C_b E_o$) and a motional component ($I_{mot} = E_o/R_Y$), where E_o is the magnitude of the driving voltage during steady-state operation. This combination is easily represented by the two-branch circuit in figure A-1 (in appendix A) to the right of terminals a and b. Since the components of the input current are in quadrature at resonance, and since the magnitude of the input current was the quantity measured during the experimental phase of the program, the relationships depicted in figure B-1 will be used to determine the motional component of the current. From figure B-1 it is obvious that

$$\left|I_{mot}\right| = \left|I\right| \left\{ 1 - \left| \frac{I_b}{I} \right|^2 \right\}^{1/2} , \qquad \text{(B-5)}$$

and that

$$\tan \Theta = \frac{|I_b|}{|I_{mot}|} . \qquad \text{(B-6)}$$

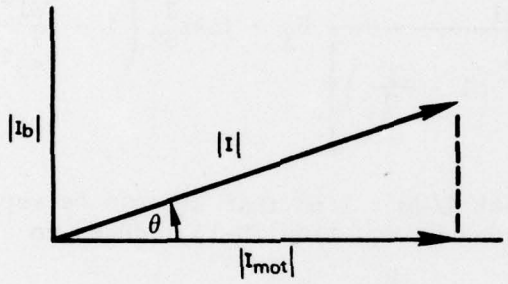

Figure B-1. Components of the Input Current at $f = f_r^E$

Now, the blocked component of the input current varies directly with the applied voltage, equation (B-4) (that is, $|I_b| = \omega_r^E C^F (1 - k^2) E_o$,* where C^F is the low frequency capacitance of the rings). Therefore, the maximum correction would be associated with the highest field level used. For ring A at a field of $E_3 = 12.5$ kV/m,

$$I_b = 2\pi(18.374 \times 10^3)(890 \times 10^{-12})(125)(1.27) = 16.3 \text{ mA}. \qquad \text{(B-7)}$$

The measured input current at the same field level is I = 239 mA, which yields a ratio of $|I_b|/|I| = 0.068$, or $|I_{mot}| = (0.998)|I|$; this value indicates that the blocked component of the input current may be neglected for all practical purposes in this report.

---

*Although C^F is known to increase with increased electric field level, the field levels during these experiments were considered to be sufficiently low that the capacitance remained essentially constant.

INITIAL DISTRIBUTION LIST

Addressee	No. of Copies
ONR, Code 412-3, 480, 410, 471 (Dr. A. M. Diness (3))	6
CNO, OP-098	1
CNM, MAT-03, -03L4	2
NRL (2), Code 6360 (P Smith, R. Pohanka), (I. Groves, R Timme)	6
NAVSEASYSCOM, SEA-06H1, -06H1-1, -06H1-2, -06H12 (C. Walker), -09G3 (4)	8
DTNSRDC	1
NAVCOASTSYSLAB	1
NUC (G. Martin)	1
NAVPGSCOL	1
DDC, Alexandria	12
ONR Boston, 495 Summer Street, Boston, MA 02210 (F. Gardner)	1
International Transducer Corp., Santa Barbara, CA 93105, P.O. Box 3385 (T. Madison)	1
Channel Products Inc., 16722 Park Circle Drive West, Chagrin Falls, OH, 44022 (D. Berlincourt)	1
Honeywell Ceramics Center, 1885 Douglas Drive, Minneapolis, MN 55422 (B. Harrison)	1
Professor L. E. Cross, Materials Research Laboratory, Pennsylvania State University, University Park, PA 16802	2
Professor D. H. Whitmore, Department of Metallurgy, Northwestern University, Evanston, IL 60201	1
Professor D. Turnbull, Divison of Engineering & Applied Science, Harvard University, Pierce Hall, Cambridge, MA 02100	1
Professor G. R. Miller, Department of Ceramic Engineering, University of Utah, Salt Lake City, UT 84112	1
Dr. Philip L. Farnsworth, Materials Department, Battelle Northwest, P.O. Box 999, Richland, WA 99352	1
Mr. E. P Eer Nisse, Ceramic Division, Sandia Corp., Albuquerque, NM 87101	1
Professor T. A Litovitz, Physics Department, Catholic University of America, Washington, DC 20017	1
Dr. Harold Liebowitz, Dean of Engineering, George Washington University, Washington, DC 20006	1

INITIAL DISTRIBUTION LIST (Cont'd)

Addressee	No. of Copies
Professor A. H. Heuer, Case Western Reserve University, University Circle, Cleveland, OH 44106	1
Dr. F. A. Kroger, University of Southern California, University Park, Los Angeles, CA 90007	1
Stanford University, Department of Material Sciences, Stanford, CA 94305	1
Professor R. W. Gould, Department of Metallurgical and Materials Engineering, College of Engineering, University of Florida, Gainesville, FL	1
Professor V. S. Stubican, Department of Material Sciences, Ceramic Science Section, Pennsylvania State University, University Park, PA 16802	1
Professor M. H. Manghnani, University of Hawaii, Hawaii Institute of Geophysics, 2525 Correa Road, Honolulu, HI 96822	1